Stabilization of unsteady flows by reduced-order control with optimally time-dependent modes

Antoine Blanchard and Themistoklis P. Sapsis

Stabilization of Unsteady Flows by
Reduced-Order Control with Optimally Time-Dependent Modes

Antoine Blanchard* and Themistoklis P. Sapsis†

Department of Mechanical Engineering, Massachusetts Institute of Technology, Cambridge, MA 02139

In dynamical systems theory, suppression of instabilities around a fixed point is generally achieved by controlling the linearized dynamics of infinitesimal perturbations, because considering small-amplitude disturbances allows for application of a range of celebrated techniques from linear control theory. In this paper, we consider the problem of design and implementation of a controller for fully nonlinear, high-dimensional, dynamical systems with the goal of steering trajectories to an unstable fixed point of the governing equations. Our control strategy is based on previous work by the authors [Blanchard, Mowlavi & Sapsis, *Nonlinear Dynamics* **95**, 2745–2764 (2019)], and takes advantage of the unique properties of the optimally time-dependent (OTD) modes, a set of global, time-evolving, orthonormal modes that track directions in phase space associated with transient growth and persistent instabilities. We show that the OTD control strategy introduced previously is robust with respect to perturbation amplitude even in cases in which the trajectory initially evolves on an attractor that lies far away from the target fixed point. In recognition of the fact that actuation capabilities are generally limited in practice, we also formulate a localized control strategy in which the OTD modes are computed in a spatially localized subdomain of the physical domain of interest. We suggest a strategy for selecting the optimal control domain based on a quantitative criterion derived from the OTD modes. We show that even when the range of the controller is reduced, OTD control is able to steer trajectories towards the target fixed point.

---

* E-mail for correspondence: ablancha@mit.edu
† E-mail for correspondence: sapsis@mit.edu

I. INTRODUCTION

From a practical perspective, control of dynamical systems faces at least two major challenges. The first is that of dimensionality. Nearly all engineering applications involve high- or infinite-dimensional physical models, for which designing robust, versatile controllers is prohibitively expensive because many control strategies do not scale well with the dimension of the system [1]. This pitfall is generally avoided by projecting the dynamics onto an appropriate low-dimensional subspace in which design and implementation of controllers are computationally tractable [2, 3]. Of course, the projection subspace must be selected with great care, because this choice immediately dictates the type of instabilities that the controller will be able to detect and act upon. Popular choices for model order reduction include the proper orthogonal decomposition (POD) [4] and its derivative, the balanced POD (BPOD) [5], the eigensystem realization algorithm (ERA) [6], and the dynamic mode decomposition (DMD) [7, 8]. However, all of these techniques have been found to struggle greatly with capturing transient (non-normal) instabilities. As noted by Rowley & Dawson [3], POD is virtually useless in situations dominated by transient growth, while DMD, BPOD, and ERA perform slightly better but still require relatively large subspaces to achieve acceptable errors, even for geometries as simple as plane Poiseuille flow. So the question remains of finding an appropriate low-dimensional subspace that most accurately capture instabilities, regardless of the exponential or non-normal nature of the latter.

The second challenge is that of nonlinearity. The general approach to flow control is based on linearization of the governing equations around an unstable fixed point, since the linearized equations describe the fate of infinitesimal perturbations in the vicinity of that fixed point [9]. Linearity is convenient because many instability and transition phenomena in fluid mechanics arise from a linear mechanism [10, 11], and also because it allows for use of an arsenal of control algorithms (e.g., optimal linear quadratic regulators or robust $\mathcal{H}_\infty$ controllers) that have been tried and tested over the years [2]. Yet, there are a number of practical situations in which the dynamics are fundamentally nonlinear and use of linear control theory is moot—for example, in control of turbulent flow [12]. In those situations, the issue of nonlinearity adds to that of high dimensionality, and it becomes much more difficult to design and implement optimal controllers that are as flexible and powerful as those available in the linear setting. Great strides have been made by using iterative, adjoint-based, gradient optimization strategies and model predictive control [13], but the underlying computational machinery is quite complex for implementation in real-life configurations. Another approach, suggested by Bewley [14], is to bluntly apply any *linear* control strategy to the corresponding fully nonlinear problem. As discussed in [14], there is some evidence that linear control strategies applied to nonlinear systems might be effective, although cases exist in which this approach has a destabilizing effect on the dynamics, rather than a stabilizing one.

The present work builds on the results of Blanchard et al. [15], who recently proposed a control strategy that addresses the first of the above challenges. Their approach leveraged the power of the optimally time-dependent (OTD) modes, a set of orthonormal basis functions that *adaptively* track directions of transient and persistent instabilities along a given trajectory of a dynamical system. This fundamental property of the OTD modes led Blanchard et al. [15] to realize that these modes formed the ideal candidate subspace for the formulation of a reduced-order control algorithm capable of suppressing transient and asymptotic instabilities. Using the fact that the OTD-reduced linearized dynamics describes the evolution of perturbations along a given trajectory with no error (i.e., there is a one-to-one correspondence between the OTD-reduced linearized system and the full-order one), they designed a controller in the OTD-reduced space that enforced no instantaneous growth of perturbations at all times. The resulting control law fulfilled the requirement of low-dimensionality (the number of control inputs equaled the number of OTD modes used in the dimensionality reduction), and was able to suppress normal and non-normal instabilities, a feat that no other reduced-order method so far had been found capable of.

The purpose of the present paper is two-fold. First, it addresses the question of robustness of the OTD control strategy proposed by Blanchard et al. [15] with respect to the amplitude of the perturbations. While the original approach relied on the assumption that perturbations around the target fixed point had small amplitude, here we consider cases in which the initial deviation from the fixed point has finite amplitude, so nonlinear effects may no longer be ignored. The goal is to determine whether OTD control, owing to its time-dependent, adaptive properties, can pull out a trajectory that initially evolves on an attractor presumably far away from the target fixed point, and drive it to an unstable fixed point of the governing equations. Second, we investigate how the control strategy by Blanchard et al. [15] can be adapted for use in situations in which range of actuation is limited, as is the case in experiments. We formulate a modified control law in which the OTD modes (and, consequently, the control force) are computed in a localized region of the physical domain in which computations or experiments are performed. We also suggest a strategy for selection of the OTD control subdomain, which we apply to various examples of high-dimensional bluff-body flows.

The paper is organized as follows. We formulate the control problem and review the concept of OTD control in §II, investigate how OTD control performs in fully nonlinear situations in §III, propose a spatially localized OTD control strategy in §IV, and offer some conclusions in §V.

II. FORMULATION OF THE PROBLEM

A. Preliminaries

We consider a finite-dimensional autonomous dynamical system

$$\dot{\mathbf{z}} = \mathbf{F}(\mathbf{z}), \quad \mathbf{z}(t_0) = \mathbf{z}_0, \tag{1}$$

where $\mathbf{z}(t) \in \mathbb{R}^d$ is the state vector at time t, $\mathbf{F} : \mathbb{R}^d \to \mathbb{R}^d$ is a smooth vector field, and overdot denotes differentiation with respect to time. Equation (1) may be viewed as the result of projecting an infinite-dimensional dynamical system onto a finite-dimensional subset of complete functions (e.g., Fourier modes or Lagrange polynomials), so the assumption of finite-dimensionality does not restrict the scope of the analysis. We assume that the dimension d of the state vector is very large, as is often the case in fluid mechanics where $\mathbf{z}$ may contain values of the primary variables (or combinations thereof) at thousands or millions of grid points or measurements points. We also assume that (1) admits at least one fixed point $\mathbf{z}_e$ (with $\mathbf{F}(\mathbf{z}_e) = \mathbf{0}$), and focus on cases in which $\mathbf{z}_e$ is linearly unstable. (Here and in what follows, the subscript e stands for "equilibrium".) Trajectories initiated in the vicinity of $\mathbf{z}_e$ are rapidly expelled from it and ultimately settle into a different attractor $\mathscr{A}$, which may be steady, time-periodic, quasi-periodic, or chaotic.

Now, we consider the controlled system

$$\dot{\mathbf{z}} = \mathbf{F}(\mathbf{z}) + \mathbf{B}\mathbf{c}, \tag{2}$$

where $\mathbf{c} \in \mathbb{R}^p$ is the control variable and $\mathbf{B} \in \mathbb{R}^{d \times p}$ is the control action matrix. *Our goal is to design the control force* $\mathbf{f}_c = \mathbf{B}\mathbf{c}$ *so that it pulls the trajectory out of the long-time attractor $\mathscr{A}$ and steers it toward the unstable fixed point* $\mathbf{z}_e$. Many challenges immediately arise, the first of which being that of dimensionality. As discussed in §I, designing a controller for (2) for a range of parameters is a very expensive task, and for the approach to be computationally tractable, order reduction of the dynamics is almost inevitable. This is usually accomplished by a Galerkin projection of (2) onto an appropriate basis. Selection of the projection basis must be done carefully, as it determines which information is retained, and which is lost upon projection. For instance, one may elect to project the governing equations onto a set of POD modes computed from a collection of snapshots of the trajectory. The resulting low-dimensional system accurately captures the dynamics encapsulated in the data used to generate it, but it is generally incapable of describing regimes for which few or no snapshots were collected [3, 16]. In fact, nearly all data-driven order-reduction techniques suffer greatly from this shortcoming, which is a simple consequence of the fact that these methods are "biased" toward the data. Likewise, the eigenvectors of the linearized operator $\mathbf{L}_e = \nabla \mathbf{F}(\mathbf{z}_e)$ have shown their limitations when it comes to model order reduction, since they fail to capture episodes of transient instabilities due to non-normal growth, a phenomenon ubiquitous in fluid mechanics and climate dynamics [17].

By contrast, our control problem requires a projection subspace that can *self-adapt* to the direction of instabilities as the trajectory evolves in the phase space. In the quest for the ideal subspace, a recent concept, introduced by Babaee & Sapsis [18] and referred to as the "optimally time-dependent (OTD) modes", has come to the rescue. The idea is to consider the evolution of a collection of r independent infinitesimal perturbations $\mathbf{v}_i \in \mathbb{R}^d$ around a given trajectory $\mathbf{z}$. Each perturbation obeys the variational equation

$$\dot{\mathbf{v}}_i = \mathbf{L}(\mathbf{z})\mathbf{v}_i, \quad 1 \leq i \leq r, \tag{3}$$

where $\mathbf{L}(\mathbf{z}) = \nabla \mathbf{F}(\mathbf{z}) \in \mathbb{R}^{d \times d}$ is the Jacobian matrix of $\mathbf{F}$ evaluated at $\mathbf{z}$. We emphasize that $\mathbf{L}(\mathbf{z})$ is a time-dependent operator because it depends on the current state $\mathbf{z}(t)$. Thus, $\mathbf{L}(\mathbf{z})$ is *not* equal to $\mathbf{L}_e$, except when $\mathbf{z} = \mathbf{z}_e$. As discussed in Wolfe et al. [19] and Blanchard & Sapsis [20], the collection of vectors $\{\mathbf{v}_i(t)\}_{i=1}^r$ propagated with (3) asymptotically collapses upon itself because the magnitude of the individual members $\mathbf{v}_i(t)$ grows exponentially rapidly, and the angle between each of them precipitously vanishes as each $\mathbf{v}_i(t)$ seeks out the most unstable direction in the phase space. To keep track of the directions associated with growth or decay of perturbations, Babaee & Sapsis [18] suggested to append to the variational equation a constraint enforcing orthonormality of the vectors $\mathbf{v}_i(t)$ at all times. Incorporating this constraint in (3) leads to the OTD equation for the ith OTD mode $\mathbf{u}_i \in \mathbb{R}^d$,

$$\dot{\mathbf{u}}_i = \mathbf{L}(\mathbf{z})\mathbf{u}_i - \sum_{k=1}^r \left(\langle \mathbf{L}(\mathbf{z})\mathbf{u}_i, \mathbf{u}_k \rangle - \Phi_{ik} \right) \mathbf{u}_k, \quad 1 \leq i \leq r, \tag{4}$$

where $\langle \cdot, \cdot \rangle$ is a suitable inner product, and $\boldsymbol{\Phi} = (\Phi_{ik})_{i,k=1}^r \in \mathbb{R}^{r \times r}$ is any skew-symmetric tensor. The subspace spanned by the collection $\{\mathbf{u}_i(t)\}_{i=1}^r$ of OTD modes is referred to as the OTD subspace, and by construction is the same as that spanned by $\{\mathbf{v}_i(t)\}_{i=1}^r$. (The OTD modes form an orthonormal basis of that subspace.) The second

term on the right-hand side of (4) sums up contributions from the Lagrange multipliers enforcing orthogonality of $\mathbf{u}_i$ and $\mathbf{u}_j$ ($i \neq j$) and normality of $\mathbf{u}_i$. Without this term, the ith OTD equation reduces to the ith variational equation (3). We emphasize that the linearized operator appearing in (4) depends on the state $\mathbf{z}$ of the system as the trajectory wanders through the phase space, which allows for the possibility of the OTD modes departing significantly from the most unstable eigendirections of $\mathbf{L}_e$. If the skew-symmetric (but otherwise arbitrary) tensor $\boldsymbol{\Phi}$ is chosen as

$$\Phi_{ik} = \begin{cases} -\langle \mathbf{L}(\mathbf{z})\mathbf{u}_k, \mathbf{u}_i \rangle, & k < i, \\ 0, & k = i, \\ \langle \mathbf{L}(\mathbf{z})\mathbf{u}_i, \mathbf{u}_k \rangle, & k > i, \end{cases} \tag{5}$$

then the OTD equations assume a lower triangular form,

$$\dot{\mathbf{u}}_i = \mathbf{L}(\mathbf{z})\mathbf{u}_i - \langle \mathbf{L}(\mathbf{z})\mathbf{u}_i, \mathbf{u}_i \rangle \mathbf{u}_i - \sum_{k=1}^{i-1} \left(\langle \mathbf{L}(\mathbf{z})\mathbf{u}_i, \mathbf{u}_k \rangle + \langle \mathbf{L}(\mathbf{z})\mathbf{u}_k, \mathbf{u}_i \rangle \right) \mathbf{u}_k. \tag{6}$$

As discussed in Blanchard & Sapsis [20], the lower triangular formulation (6) is particularly insightful because it is equivalent to continuously performing Gram–Schmidt orthonormalization on $\{\mathbf{v}_i(t)\}_{i=1}^r$, starting with $\mathbf{v}_1(t)$ and moving down. This is the approach we will use to generate the numerical results presented in §IV.

Why are the OTD modes relevant to our reduced-order control problem? To answer this, we must first review some of the properties of the OTD modes. The fact that the OTD modes span the same subspace as the solutions of (3) implies that an r-dimensional OTD subspace constantly seeks out the most rapidly growing r-dimensional subspace in the tangent space (i.e., the space of perturbations). For example, for a hyperbolic fixed point, the most rapidly growing subspace is the unstable eigenspace of the associated linearized operator, and it has been shown that the OTD subspace precisely aligns with that subspace at long times [18]. For a time-dependent trajectory, the OTD subspace aligns exponentially fast with the most unstable eigenspace of the left Cauchy–Green tensor (i.e., the eigenspace associated with transient instabilities) [21], just like any subspace solution of (3). In other words, the OTD modes essentially *track* the directions in the phase space along which transient and persistent instabilities develop. The added constraint of orthonormality is key, as it provides a numerically stable way of computing those directions (the OTD subspace does not collapse on itself).

In light of this, it is natural to consider the OTD modes as a candidate basis to reduce the dimensionality of the linearized dynamics. We introduce the matrix $\mathbf{U} \in \mathbb{R}^{d \times r}$ whose ith column is $\mathbf{u}_i$, and note that for any solution $\mathbf{v}$ of the variational equation (3) that belongs to the OTD subspace, the projection

$$\boldsymbol{\eta}(t) = \mathbf{U}(t)^{\mathsf{T}} \mathbf{v}(t) \in \mathbb{R}^r \tag{7}$$

(where T denotes the Hermitian transpose operator) obeys the reduced linear equation

$$\dot{\boldsymbol{\eta}} = \mathbf{L}_r \boldsymbol{\eta}, \tag{8}$$

where we have introduced the reduced linear operator

$$\mathbf{L}_r = \mathbf{U}^{\mathsf{T}} \mathbf{L}(\mathbf{z}) \mathbf{U} + \boldsymbol{\Phi}. \tag{9}$$

The dimensionality of (8) is the same as that of the OTD subspace, and presumably much smaller than that of the original equation (3). A great advantage of the OTD order reduction is that it is *dynamically consistent*, i.e., if $\boldsymbol{\eta}$ solves the reduced equation (8), then $\mathbf{v} = \mathbf{U}\boldsymbol{\eta}$ solves the original equation (3), and *vice versa* [22]. This means that propagating $\mathbf{v}$ with (3) is strictly equivalent to propagating $\boldsymbol{\eta}$ with (8) and projecting the solution back to the full space. Thus, the OTD reduction consistently retains the information of the full-order system associated with transient instabilities along an evolving trajectory. For this reason, the OTD framework is particularly appropriate for design of low-dimensional controllers. This was recognized by Blanchard et al. [15], who were the first to propose an OTD-based control algorithm with a view to suppressing modal and non-modal growth around fixed points in high-dimensional systems. Their approach will be the basis for our analysis, so we briefly review it below.

B. Review of control by optimally time-dependent modes

To formulate an OTD-based control law, Blanchard et al. [15] considered the controlled dynamics of an infinitesimal perturbation $\mathbf{z}' \in \mathbb{R}^d$ around a fixed point $\mathbf{z}_e$, described by

$$\dot{\mathbf{z}}' = \mathbf{L}\mathbf{z}' + \mathbf{B}\mathbf{c}, \tag{10}$$

where $\mathbf{L} \equiv \mathbf{L}(\mathbf{z})$ is used as a proxy for $\mathbf{L}_e$. Introducing the OTD projection $\boldsymbol{\eta} = \mathbf{U}^\mathsf{T}\mathbf{z}'$, and defining a reduced control matrix $\mathbf{B}_r = \mathbf{U}^\mathsf{T}\mathbf{B} \in \mathbb{R}^{r \times p}$, they obtained the reduced controlled variational equation

$$\dot{\boldsymbol{\eta}} = \mathbf{L}_r\boldsymbol{\eta} + \mathbf{B}_r\mathbf{c}. \tag{11}$$

If the control vector is sought in the form $\mathbf{c} = \mathbf{K}_r\boldsymbol{\eta}$, with $\mathbf{K}_r \in \mathbb{R}^{p \times r}$ a reduced feedback gain matrix, then (11) reduces to

$$\dot{\boldsymbol{\eta}} = \mathbf{L}_{r,c}\boldsymbol{\eta}, \tag{12}$$

where $\mathbf{L}_{r,c} = \mathbf{L}_r + \mathbf{B}_r\mathbf{K}_r$ is the closed-loop reduced linear operator. The latter is time-dependent, so its eigenvalues are not good indicators for growth or decay of $\|\boldsymbol{\eta}\|$. However, the eigenvalues of its symmetric part characterize the instantaneous rate of change of the magnitude of the reduced perturbation, since

$$\frac{1}{2}\frac{\mathrm{d}}{\mathrm{d}t}\|\boldsymbol{\eta}\|^2 = \frac{\langle\mathbf{L}_{r,c}\boldsymbol{\eta}, \boldsymbol{\eta}\rangle + \langle\boldsymbol{\eta}, \mathbf{L}_{r,c}\boldsymbol{\eta}\rangle}{2}. \tag{13}$$

To stabilize the fixed point $\mathbf{z}_e$, Blanchard et al. [15] required that the magnitude of reduced perturbations always decay (i.e., $\mathrm{d}\|\boldsymbol{\eta}\|^2/\mathrm{d}t < 0$ for all $\boldsymbol{\eta} \neq \mathbf{0}$) and, hence, that $(\mathbf{L}_{r,c} + \mathbf{L}_{r,c}^\mathsf{T})/2$ be negative definite. They noted, however, that there is no general framework in control theory addressing the issue of pole placement for the *symmetric part* of a linear operator. So they made one additional assumption, namely, that the controller can act on every state of the system (i.e., $\mathbf{B} = \mathbf{I}$) and, invoking dynamical consistency of the OTD reduction, arrived at a rather simple *ad hoc* expression for the control force,

$$\mathbf{f}_c = \mathbf{U}\mathbf{Q}\mathrm{diag}[-(\lambda_i + \zeta)\mathscr{H}(\lambda_i)]\mathbf{Q}^\mathsf{T}\mathbf{U}^\mathsf{T}(\mathbf{z} - \mathbf{z}_e), \tag{14}$$

where $\mathscr{H}$ is the Heaviside function, $\zeta \in \mathbb{R}^+$ is a damping parameter, $\mathbf{Q} \in \mathbb{R}^{r \times r}$ is a unitary rotation matrix containing the eigenvectors of $(\mathbf{L}_r + \mathbf{L}_r^\mathsf{T})/2$, and $\{\lambda_i\}_{i=1}^r$ are the eigenvalues of $(\mathbf{L}_r + \mathbf{L}_r^\mathsf{T})/2$ ranked from most (λ_1) to least (λ_r) unstable. The Heaviside function guarantees that the control acts only on directions associated with positive instantaneous growth (those with $\lambda_i \geq 0$), and the parameter ζ governs the intensity with which these directions are damped. The closed-loop rate of change of $\|\boldsymbol{\eta}\|$ is thus negative for all times, thereby ensuring that $\mathbf{z}$ tends to $\mathbf{z}_e$ asymptotically. Due to orthonormality of the OTD modes, the input energy required by the control law (14) can be easily computed as

$$E_c = \int_{t_a}^\infty \|\mathbf{U}^\mathsf{T}\mathbf{f}_c\|^2\mathrm{d}\tau, \tag{15}$$

where t_a denotes the time at which OTD control is activated. There is, of course, an additional cost related to computation of the OTD modes, which involves solving r d-dimensional differential equations (i.e., the OTD system (6)). Babaee et al. [21] showed that, in the context of computation of finite-time Lyapunov exponents, the cost of evolving the OTD equations becomes insignificant as the dimension d of the system becomes large.

As discussed in Blanchard et al. [15], the control law (14) guarantees suppression of transient and asymptotic instabilities around $\mathbf{z}_e$ provided that the following three requirements are met. First, for the order reduction to be dynamically consistent, the OTD subspace must be initialized so that it contains the directions in which the initial deviation $\mathbf{z}(t_0) - \mathbf{z}_e$ grows. Short of this condition (e.g, if the deviation is initially orthogonal to the OTD subspace), the reduced-order system (11) will leave out some or all of the directions associated with instabilities, on which the control force (14) will thus have no influence. The second prerequisite is that the dimension r of the OTD subspace be sufficiently large that no information related to instability is lost upon order reduction. To capture both normal and non-normal instabilities, Blanchard et al. [15] suggested to select r according to

$$r \geq \max(\dim\mathcal{E}_u, \dim\mathcal{E}_u^s), \tag{16}$$

where $\mathcal{E}_u$ and $\mathcal{E}_u^s$ are the unstable eigenspace of $\mathbf{L}_e$ and $(\mathbf{L}_e + \mathbf{L}_e^\mathsf{T})/2$, respectively. Criterion (16) pertains to the full-order operators evaluated at the fixed point $\mathbf{z}_e$, so it relies on the assumption that the norm of the perturbation $\mathbf{z} - \mathbf{z}_e$ never becomes excessively large. This assumption constitutes the third requirement identified by Blanchard et al. [15]. It allowed use of $\mathbf{L}$ as a proxy for $\mathbf{L}_e$ in (10), and made consistent application of (14) to the original nonlinear equation (2), notwithstanding that (14) was designed based on the dynamics of the variational equation (10). (These manipulations are valid if $\|\mathbf{z} - \mathbf{z}_e\|$ remains relatively small.)

In the following exposition, we address two key issues raised by Blanchard et al. [15]. The first question is that of robustness of the control with respect to the amplitude of the perturbation. Success of the control strategy (14) is guaranteed for small perturbations around $\mathbf{z}_e$, but it is not clear whether OTD control ceases to work for

disturbances with finite amplitude. After all, the OTD modes are able to capture directions of instabilities along any given trajectory, regardless of how far the state $\mathbf{z}$ may be from $\mathbf{z}_e$. So it might very well be that the control algorithm performs extremely well even in situations where linearization is *a priori* not valid. Robustness is important because controllers usually "shift" the attractor significantly, rendering models based on POD modes, DMD modes, or eigenvectors (which are "local" in phase space) moot. Thus, designing a reduced-order controller that is robust to perturbation amplitude and direction is often considered a daunting task. The results presented hereinafter will make clear that the OTD modes significantly "deform" as the magnitude of the perturbation grows, which is a key requirement for robustness of the proposed control algorithm.

The second issue has to do with the range of the control force. In the original formulation, the controller took the form of a body force acting on the entire physical domain (cf. equation (14)). As noted by Blanchard et al. [15], it would be valuable to design a control law that acts only in part of the physical domain, because this would make the approach considerably more attractive from the standpoint of conducting experiments.

III. STABILIZATION OF UNSTEADY FLOWS BY OTD CONTROL

In this section, we investigate how robust the control law (14) is to the amplitude of the perturbation. We apply the control algorithm (with minor modifications discussed below) to cases in which the initial deviation of the trajectory from $\mathbf{z}_e$ is not small. Specifically, we investigate whether OTD control is able to steer the trajectory toward $\mathbf{z}_e$ after it pulled it out of a long-time attractor that presumably lies far away from $\mathbf{z}_e$. In what follows, the control force is assumed to act on the entire physical domain, as done in the original formulation by Blanchard et al. [15]. We emphasize that the control force was designed based on the linearized dynamics, but to test its robustness we decide to apply it to the fully nonlinear equations. As discussed in §I, this approach is similar to that proposed by Bewley [14] in which linear control strategies were applied to nonlinear systems.

A. Unsteady low-dimensional nonlinear system

We begin our investigation with a simple low-dimensional nonlinear system introduced by Trefethen et al. [23],

$$\dot{\mathbf{z}} = \mathbf{Cz} + \|\mathbf{z}\|\mathbf{Dz}, \tag{17a}$$

where

$$\mathbf{C} = \begin{bmatrix} -1/R & 1 \\ 0 & -2/R \end{bmatrix}, \quad \mathbf{D} = \begin{bmatrix} 0 & -1 \\ 1 & 0 \end{bmatrix}, \tag{17b}$$

and R is a large parameter (here, $R = 25$). The matrix $\mathbf{C}$ is non-normal, so the linear term on the right-hand side of (17a) amplifies energy transiently. The nonlinear term involving the skew-symmetric matrix $\mathbf{D}$ merely redistributes energy, but neither creates nor destroys any. As discussed by Trefethen et al. [23], a notable feature of this system is that although the fixed point $\mathbf{z}_e = \mathbf{0}$ is asymptotically stable, sufficiently large non-normal amplification of a perturbation can activate nonlinear energy mixing, leading to expulsion of the trajectory from the vicinity of $\mathbf{z}_e$ and transition to a different long-time attractor. System (17a,b) essentially mimics transition to turbulence in the Navier–Stokes equations. In (17a,b), transient growth results from self-sustained transfer of energy to the principal right singular vector of the non-normal operator $\mathbf{C}$, facilitated by the nonlinear terms.

Blanchard et al. [15] showed that for a range of initial disturbances, a one-dimensional OTD subspace ($r = 1$), and damping coefficient $\zeta = 0.1$, the control force (14) was able to suppress non-normal growth around $\mathbf{z}_e = \mathbf{0}$. In their numerical experiments, the amplitudes of the initial disturbances were small (no larger than 10^{-2}), so OTD control was only used to prevent transient amplification of the disturbances and, hence, transition. Here, however, we do not wish to prevent transition, but rather attempt to steer the trajectory toward the fixed point $\mathbf{z}_e = \mathbf{0}$ *after transition has occurred* and once the trajectory is in a state presumably far from $\mathbf{z}_e$. We consider a range of initial conditions in the form $(0, c)^\mathsf{T}$ (c a constant) for which non-normal growth is large enough that it leads to transition. Integration of (17a,b) is performed with a third-order Adams–Bashforth method with time-step size $\Delta t = 0.1$. For the range of initial conditions considered, it is straightforward to show that the long-time "turbulent" attractor is actually another (linearly stable) fixed point, given by $\mathbf{z}'_e \approx (0.0797, 0.9936)^\mathsf{T}$ for $R = 25$ (cf. figure 1a).

We use the OTD control law (14) with $r = 1$ and $\zeta = 0.1$ to drive the trajectory toward $\mathbf{z}_e$ after transition has occurred. The control is activated at $t = 100$ as the trajectory is headed toward $\mathbf{z}'_e$. Figure 1b shows that the controller has no difficulty halting the approach to $\mathbf{z}'_e$. Upon activation of the control, the trajectory is swiftly ejected to a different region of the phase space, and then guided toward $\mathbf{z}_e$. Figure 1b suggests that expulsion from the

vicinity of $\mathbf{z}'_e$ happens more rapidly for initial disturbances with smaller amplitudes. This is because it takes longer for smaller disturbances to grow, so $\mathbf{z}$ is not as close to $\mathbf{z}'_e$ when the control is activated. In contrast, for disturbances with larger initial amplitudes, trajectories fall in the "radius of influence" of $\mathbf{z}'_e$ more rapidly, and it is more difficult for the controller to pull them out of it. Figure 1c shows that this effect is much less pronounced when the value of the damping coefficient ζ is increased to 0.6.
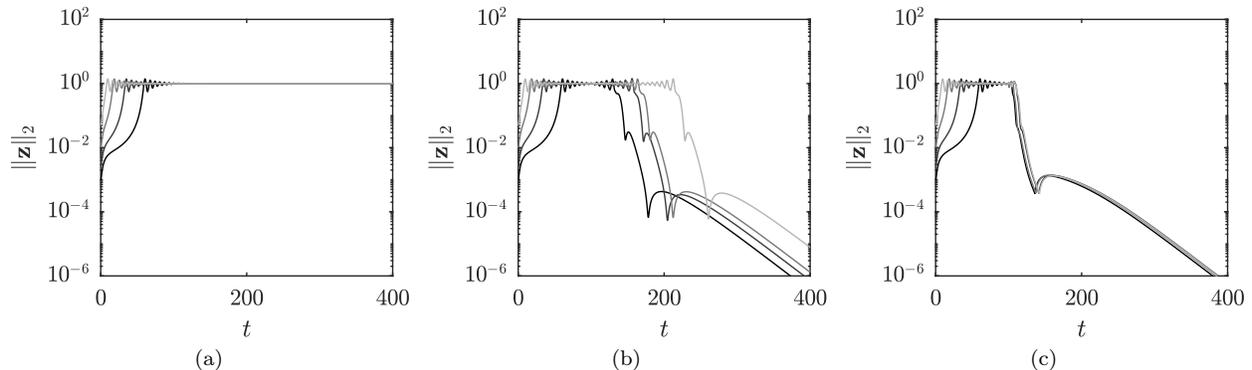
FIG. 1. For the 2-by-2 non-normal system (17a,b), norm of trajectories subject to (a) no control, (b) OTD control with $r = 1$ and $\zeta = 0.1$, and (c) OTD control with $r = 1$ and $\zeta = 0.6$. In (b) and (c), control is activated at $t = 100$. Initial conditions for the trajectories are $(0, c)^\mathsf{T}$, where $c = 10^{-3}$, 2.5×10^{-3}, 10^{-2} and 5×10^{-2}, from darker to lighter.

Figures 1b,c show that increasing the value of ζ does not accelerate the final approach to $\mathbf{z}_e$. The reason is that the the first OTD mode used in the control asymptotically aligns with the most unstable eigendirection of $\mathbf{L}_e$. Since the target fixed point is asymptotically stable, that eigendirection is associated with a negative eigenvalue. So in the limit $\mathbf{z} \to \mathbf{z}_e$, the reduced operator $\mathbf{L}_r$ (and for that matter, its symmetric part) reduces to a negative number, and the controller becomes idle. To accelerate the final approach to $\mathbf{z}_e$, one approach would be to apply damping to every OTD direction regardless of the sign of λ_i, and simultaneously increase the dimension of the OTD subspace. We will elaborate on the possibility of damping out all the OTD directions in §III B.

We note that the time at which control is activated cannot be chosen arbitrarily large, for the following reason. If the control force were to be switched on long after transition happened (i.e., when the state $\mathbf{z}$ nearly coincides with the fixed point $\mathbf{z}'_e$), OTD control would be no different from modal control, since the OTD subspace would have aligned with the most unstable eigenspace of $\mathbf{z}'_e$. If a single mode is used in the order reduction, the control would remain idle for all times because the reduced linear operator reduces to the most unstable eigenvalue of $\mathbf{L}'_e$, which is a negative number. (The case of OTD reduction with two modes is of little interest, since in that case the OTD basis spans the whole phase space.) Thus, OTD control must be activated before the asymptotic limit is reached.

We also note that if the controller were to be turned off after $\mathbf{z}$ had been driven sufficiently close to the target $\mathbf{z}_e$, non-normal instability of the latter would set in again, and two scenarios are possible. If the control is switched off when $\mathbf{z}$ is infinitesimally close to $\mathbf{z}_e$, non-normal growth of the deviation $\mathbf{z} - \mathbf{z}_e$ would not be large enough to trigger transition to $\mathbf{z}'_e$, and the trajectory would naturally return to $\mathbf{z}_e$, since the latter is asymptotically stable. On the other hand, if the controller is switched off when $\mathbf{z}$ is not infinitesimally close to $\mathbf{z}_e$, the amplitude of $\mathbf{z} - \mathbf{z}_e$ might be sufficiently amplified that transition would occur again. Should that happen, reactivation of OTD control after transition would irremediably steer the trajectory back to $\mathbf{z}_e$. This is possible because the OTD modes are able to adapt to directions of instabilities as the trajectory evolves in phase space. OTD control thus provides a mechanism for switching on and off transition at will.

B. Flow past a cylinder

We turn to the two-dimensional flow of a Newtonian fluid with constant density ρ and kinematic viscosity ν past a circular cylinder of diameter D with uniform free-stream velocity $U\mathbf{e}_x$. The Navier–Stokes equations can be written in dimensionless form as

$$\partial_t \mathbf{w} + \mathbf{w} \cdot \nabla \mathbf{w} = -\nabla p + \frac{1}{Re}\nabla^2 \mathbf{w}, \tag{18a}$$

$$\nabla \cdot \mathbf{w} = 0, \tag{18b}$$

with no-slip boundary condition

$$\mathbf{w}|_{\Gamma_{cyl}} = \mathbf{0} \tag{19a}$$

on the cylinder surface Γ_{cyl}, and uniform flow

$$\lim_{x,y \to \infty} \mathbf{w} = \mathbf{e}_x \tag{19b}$$

in the far field. Velocity, time and length have been scaled with cylinder diameter D and free-stream velocity U, and the Reynolds number is $Re = UD/\nu$. With the lower-triangular formulation discussed in §II, the ith OTD mode obeys

$$\dot{\mathbf{u}}_i = \mathbf{L}_{ns}\mathbf{u}_i - \langle \mathbf{L}_{ns}\mathbf{u}_i, \mathbf{u}_i \rangle \mathbf{u}_i - \sum_{k=1}^{i-1} \left[\langle \mathbf{L}_{ns}\mathbf{u}_i, \mathbf{u}_k \rangle + \langle \mathbf{L}_{ns}\mathbf{u}_k, \mathbf{u}_i \rangle \right] \mathbf{u}_k, \tag{20a}$$

$$\nabla \cdot \mathbf{u}_i = 0, \tag{20b}$$

with boundary conditions

$$\mathbf{u}_i|_{\Gamma_{cyl}} = \mathbf{0} \tag{21a}$$

and

$$\lim_{x,y \to \infty} \mathbf{u}_i = \mathbf{0}, \tag{21b}$$

where $\langle \cdot, \cdot \rangle$ is the usual L^2 inner product. The (spatially discretized) linearized Navier–Stokes operator evaluated at the current state $\mathbf{w}$ is given by

$$\mathbf{L}_{ns}\mathbf{u}_i = -\nabla p_i + \frac{1}{Re}\nabla^2 \mathbf{u}_i - \mathbf{w} \cdot \nabla \mathbf{u}_i - \mathbf{u}_i \cdot \nabla \mathbf{w}, \tag{22}$$

where p_i is the pressure field that guarantees incompressibility of the OTD mode $\mathbf{u}_i$.

We consider the case $Re = 50$, slightly above the Hopf bifurcation of the steady symmetric solution $\mathbf{w}_e$ known to occur at $Re_c \approx 47$. At $Re = 50$, there is exactly one pair of unstable complex conjugate eigenvalues [24, 25], which at long times gives rise to a limit cycle with periodic vortex shedding. Blanchard et al. [15] showed that for small asymmetric inlet perturbations, the control law (14) based on an OTD subspace with dimension at least 2 (and $\zeta = 0.1$) subdued linear instability of the base flow. By contrast, they showed that control law (14) with a one-dimensional OTD subspace was unable to counteract development of the vortex street. The reason is that the most unstable eigenspace of $\mathbf{L}_e$, with which the OTD subspace rapidly aligns if the flow is initialized infinitesimally close to $\mathbf{w}_e$, contains two unstable directions. Hence, a controller based on a single OTD mode necessarily leaves out one of the two directions responsible for instability.

Here, we do not use OTD control to suppress linear growth of initially small disturbances around $\mathbf{w}_e$. Rather, we investigate whether OTD control can take the trajectory out of the limit cycle and guide it toward $\mathbf{w}_e$. This may be thought of as an attempt to control an initially *non-infinitesimal* perturbation, since on the limit cycle, $\mathbf{w}$ is far from $\mathbf{w}_e$, and the nonlinearity of the Navier–Stokes equations is fully active. The question then arises of how many OTD modes should be included in the control algorithm in order to stabilize $\mathbf{w}_e$. (We chose not to discuss this issue in §III A because for that example the phase space was two-dimensional.) As discussed in §II, the original criterion (16) formulated by Blanchard et al. [15] guarantees success of the control strategy if the amplitude of the perturbation is small. Here, however, we consider perturbations that have finite amplitude, and there is no reason to believe that choosing $r = \max(\dim \mathcal{E}_u, \dim \mathcal{E}_u^s)$ should ensure success of the control strategy. But under no circumstances can r be less than $\max(\dim \mathcal{E}_u, \dim \mathcal{E}_u^s)$, since the latter accounts for exactly all the directions of transient and asymptotic instabilities of $\mathbf{w}_e$.

The computational solution is effected using the spectral-element Navier–Stokes solver `nek5000` [26]. The computational domain extends $24D$ in the cross-stream direction and $32.4D$ in the streamwise direction. The cylinder center is located $8.4D$ away from the inlet boundary and equidistantly from the side-walls. Our production runs use a mesh with 316 spectral elements, polynomial degree $N = 9$, and time-step size $\Delta\tau = 2 \times 10^{-3}$. For the main flow and the OTD modes, we specify a no-penetration ("symmetry") boundary condition on the side-walls, and a stress-free condition at the outlet. At the inlet, we prescribe a non-homogeneous Dirichlet condition ($\mathbf{w} = \mathbf{e}_x$) for the main flow, and a homogeneous Dirichlet condition for the OTD modes. The steady (unstable) base flow $\mathbf{w}_e$ shown in figure 2a is computed by a selective-frequency-damping (SFD) approach [27].
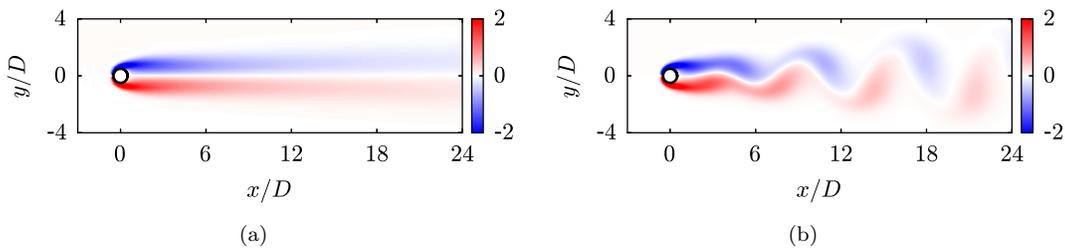
FIG. 2. For flow past a cylinder at $Re = 50$, (a) spanwise vorticity distribution of the steady symmetric solution $\mathbf{w}_e$, and (b) snapshot of the spanwise vorticity distribution of the solution on the limit cycle at an instant for which C_L is maximum.

We first perform a computation with $r = 2$ (the smallest value of r for which stabilization is possible in the limit of small perturbations) and $\zeta = 0.1$. Initial conditions for the main flow are selected as the state on the limit cycle for which the lift coefficient C_L is maximum (cf. figure 2b). For the initial conditions of the OTD modes, we apply Gram–Schmidt orthonormalization to the divergence-free subspace $\{\sin(my)\mathbf{e}_x + \cos(mx)\mathbf{e}_y\}_{m=1}^r$. (For a detailed discussion of the initialization of the OTD subspace, we refer the reader to Blanchard et al. [15].) For $0 \leq t < 100$, the control is idle, and the OTD subspace aligns with the most unstable subspace on the limit cycle. Figures 3a–h show the vorticity distributions of the first and second OTD modes at four equally-spaced time instants in one shedding cycle of period T, with C_L reaching its maximum amplitude at $t = t_0$. Figures 3a–f show that the OTD modes posses the same space-time symmetry

$$u_{i,x}(x, y, t) = u_{i,x}(x, -y, t + T/2), \tag{23a}$$
$$u_{i,y}(x, y, t) = -u_{i,y}(x, -y, t + T/2), \tag{23b}$$
$$p_i(x, y, t) = p_i(x, -y, t + T/2), \tag{23c}$$

as the flow itself [28]. This is a consequence of the fact that the OTD subspace aligns exponentially fast with a well-defined subspace that depends only on the current flow state $\mathbf{w}$, and not on the history of the trajectory [20, 29]. As a result, the OTD modes inherit the symmetry properties of the flow. Figures 3a–h also show that the vorticity distributions of the OTD modes on the limit cycle are quite different from that of the OTD modes computed at the unstable fixed point $\mathbf{w}_e$ (figures 4a,b). As discussed in §II B, the reason is that the OTD subspace evolves hand in hand with the trajectory. Thus, the OTD subspace coincides with $\mathcal{E}_u$ only in the asymptotic limit $\mathbf{w} \to \mathbf{w}_e$, but otherwise strongly departs from $\mathcal{E}_u$.

The control is activated at $t = 100$, and remains active for all $t > 100$. Figure 5a shows that the control law (14) is able to drive $\mathbf{w}$ towards $\mathbf{w}_e$. In addition, movie 1 [30] shows time series for C_L cued to the vorticity distributions of the solution $\mathbf{w}$ and the control force $\mathbf{f}_c$. Movie 1 [30] shows that the amplitude of C_L decreases by about 90% between $t = 100$ and 150, evidencing that the controller acts very rapidly. It is also clear from movie 1 [30] that the vorticity distribution of $\mathbf{f}_c$ exhibits strong asymmetry about the midline $y = 0$ for most of the transient interval during which the trajectory leaves the limit cycle and travels toward $\mathbf{w}_e$ (i.e., for about $100 \leq t \leq 145$). As $\mathbf{w}$ approaches $\mathbf{w}_e$, the vorticity distribution of the solution becomes anti-symmetric, and so does that of the control force $\mathbf{f}_c$ (see for example $t = 160$ in movie 1 [30]). At long times, $\mathbf{f}_c$ is a linear combination of the two most unstable eigenvectors of $\mathbf{L}_e$ (cf. figures 4a,b). For $t \geq 200$, the vorticity distribution of the solution is indistinguishable from that of $\mathbf{w}_e$.

A notable feature of movie 1 [30] is that there are multiple "flickers" in the vorticity distribution of the control force (e.g., near $t = 123.4$, 128.8, and 131). We have verified that these episodes should not be attributed to insufficient frame rate in movie 1 [30], as they were found to persist even when the speed of the movie was decreased by a factor of two, and the frame rate simultaneously increased by a factor of five. Instead, an explanation is provided by examining the time series for the eigenvalues $\{\lambda_1, \lambda_2\}$ of $(\mathbf{L}_r + \mathbf{L}_r^\mathsf{T})/2$, shown in figure 5b. We first recall that the control law (14) contains a Heaviside function, whose use was originally motivated by the fact that only those directions with positive instantaneous growth rate should be acted upon (and the other directions should be left unaltered). However, figure 5b shows that the two eigenvalues of $(\mathbf{L}_r + \mathbf{L}_r^\mathsf{T})/2$ have opposite signs at the time when the control is activated (with $\lambda_1 > 0 > \lambda_2$), but identical signs at long times when the trajectory is close to $\mathbf{w}_e$ (with $\lambda_1 > \lambda_2 > 0$). So λ_2 must change sign at least once as the trajectory travels from the limit cycle to the fixed point. In fact, figure 5b shows that λ_2 changes sign multiple times in the interval $120 \leq t \leq 170$ (at $t = 123.54$, 123.75, 127.26, 128.81, 131.09, and again at $t = 164.55$ and 164.92). These time instants coincide with the "flickers" in the vorticity distribution of $\mathbf{f}_c$: every time λ_2 becomes positive, OTD mode 2 is suddenly included in the control force, and its contribution "jumps" from zero to non-zero. (Likewise, when λ_2 becomes negative, OTD mode 2 is suddenly excluded from $\mathbf{f}_c$.)

There are at least two options to eliminate temporal discontinuities in the control force. One possibility is to
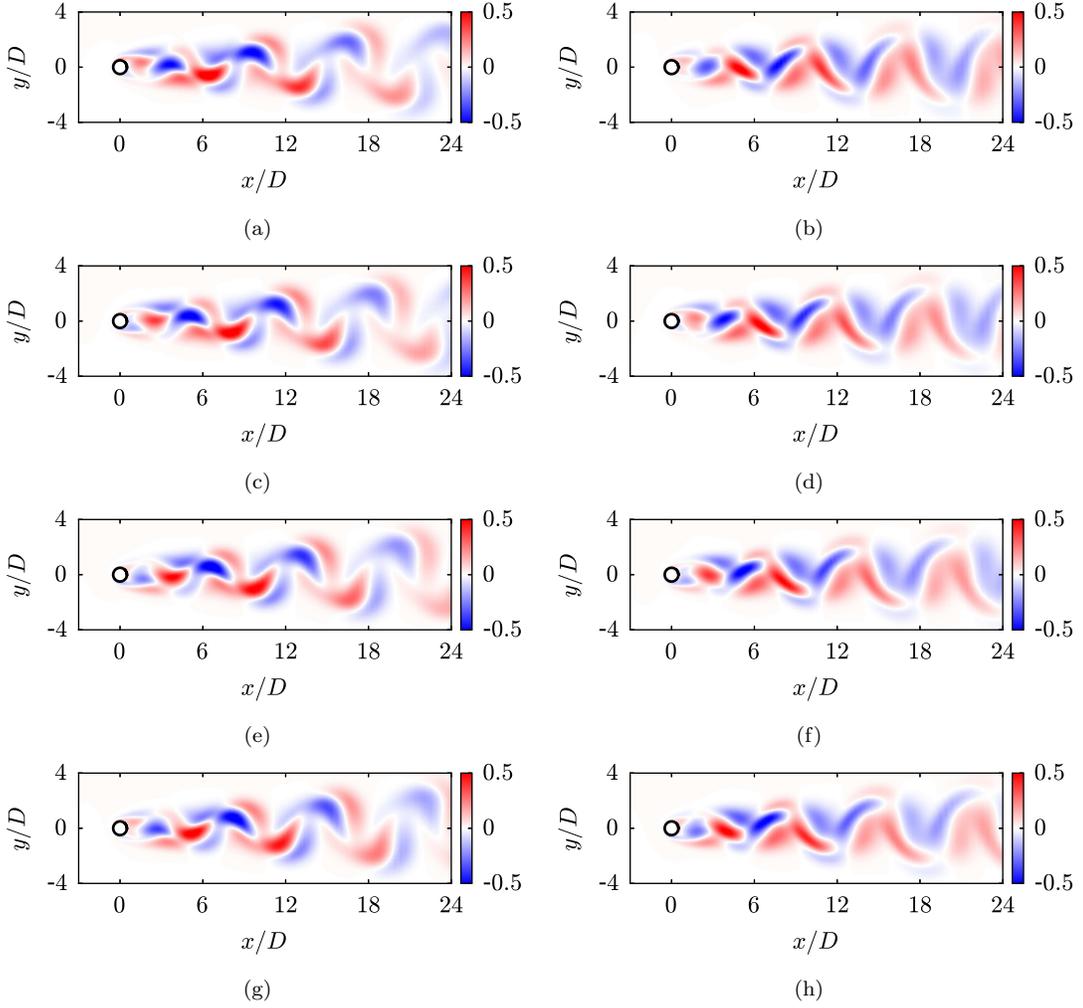
FIG. 3. For flow past a cylinder at $Re = 50$ on the limit-cycle attractor, vorticity distributions of the (a, c, e, g) first and (b, d, f, h) second OTD mode, shown at time (a, b) t_0, (c, d) $t_0 + T/4$, (e, f) $t_0 + T/2$, and (g, h) $t_0 + 3T/4$.
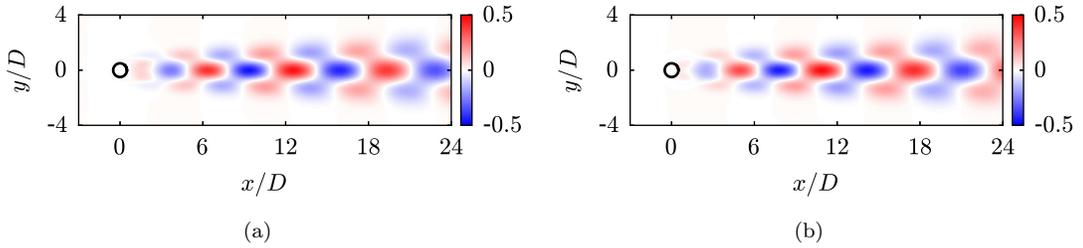
FIG. 4. For the steady (unstable) flow past a cylinder at $Re = 50$, vorticity distributions of the (a) first and (b) second OTD mode.

introduce an offset $\varepsilon > 0$ in (14), so that $\mathbf{f}_c$ becomes

$$\mathbf{f}_{c,\varepsilon} = \mathbf{U}\mathbf{Q}\text{diag}[-(\lambda_i + \zeta)\mathscr{H}(\lambda_i + \varepsilon)]\mathbf{Q}^{\mathsf{T}}\mathbf{U}^{\mathsf{T}}(\mathbf{z} - \mathbf{z}_e). \tag{24}$$

The modified control law (24) damps out directions of instantaneous growth (just like (14)), as well as those directions that instantaneously decay at a rate smaller than ε. In other words, for small values of ε, (24) damps out directions along which perturbations grow or barely decay. Temporal discontinuities in $\mathbf{f}_c$ are eliminated if $\lambda_i + \varepsilon$ never changes sign. In practice, however, it is difficult to know in advance how each λ_i will evolve when the control is active. So another approach is to simply eliminate the Heaviside function from (14), and apply the same amount of damping to
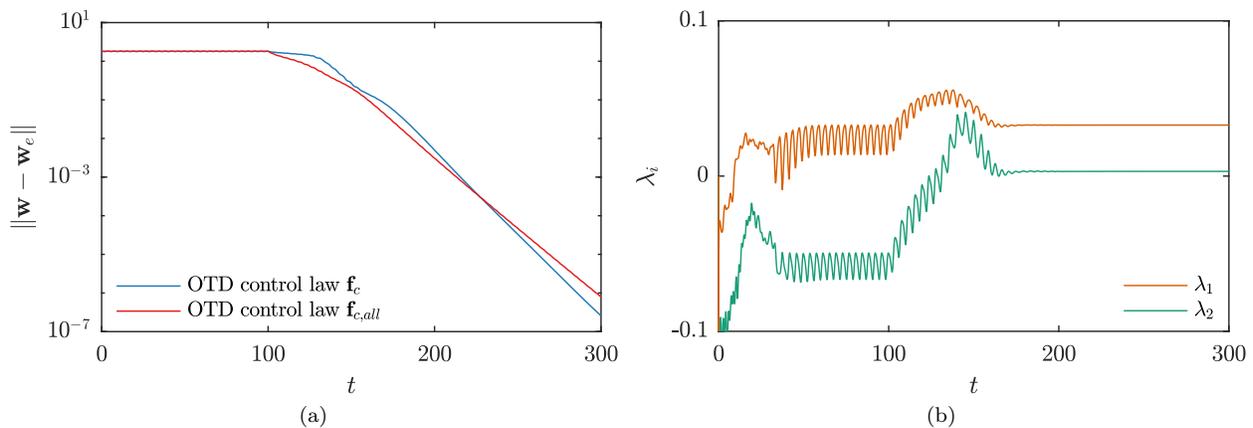
FIG. 5. For flow past a cylinder at $Re = 50$ subject to OTD control with $r = 2$ and $\zeta = 0.1$, (a) time series of $\|\mathbf{w} - \mathbf{w}_e\|$, and (b) eigenvalues of the open-loop reduced operator $(\mathbf{L}_r + \mathbf{L}_r^\mathsf{T})/2$. Control is idle in the interval $0 \leq t < 100$ and active for $t \geq 100$.

every OTD direction, regardless of whether it is associated with instantaneous growth or decay:

$$\mathbf{f}_{c,all} = \mathbf{UQ}\mathrm{diag}(-\zeta)\mathbf{Q}^\mathsf{T}\mathbf{U}^\mathsf{T}(\mathbf{z} - \mathbf{z}_e). \tag{25}$$

The above control strategy is suboptimal, since resources are allotted to damping directions that need not be, but it guarantees temporal continuity of the control force at all times. We note that with this strategy, the damping coefficient ζ must be chosen sufficiently large that it can suppress the leading eigenvalue λ_1. Figure 5a shows that use of (25) with $\zeta = 0.1$ is able to stabilize $\mathbf{w}_e$, and movie 2 [30] confirms that no temporal discontinuities are present in $\mathbf{f}_{c,all}$. For this control strategy, the input energy E_c required to operate the controller is found to be 0.132, slightly lower than that for the case shown in movie 1 (0.180).

C. Flow past a NACA 0012 airfoil

For another example of control of bluff-body flow, we consider the two-dimensional flow of an incompressible fluid with density ρ, kinematic viscosity ν, and free-stream velocity $U\mathbf{e}_x$, past a NACA 0012 airfoil of chord length L_c at an angle of attack $\alpha = 10°$. The governing equations and boundary conditions for the main flow and the OTD modes are identical to (18a–22), where it is understood that Γ_{cyl} now denotes the airfoil surface. The Reynolds number, based on the chord length, is $Re = UL_c/\nu$. The Navier–Stokes and OTD equations are solved using `nek5000`. The computational domain is a C-grid that extends $10L_c$ in the streamwise direction and $8L_c$ in the cross-stream direction. The airfoil trailing edge is located $5L_c$ from the outlet boundary and equidistantly from the side-walls. The mesh is composed of 644 spectral elements with polynomial order $N = 9$, and the time-step size is $\Delta\tau = 5 \times 10^{-4}$. The computational boundary conditions for the main flow and the OTD modes are identical to those used in §III B.

Like in the cylinder flow discussed in §III B, the equations governing flow past a NACA 0012 airfoil admit a steady solution $\mathbf{w}_e$ for any value of Re and α. The only case for which $\mathbf{w}_e$ is symmetric about the midline $y = 0$ is when the geometry is symmetric, i.e., for $\alpha = 0°$. For $Re = 1000$, Kurtulus [31] found that $\mathbf{w}_e$ loses linear stability at $\alpha_c \approx 8°$. For $Re = 1000$ and α not too greater than α_c, there is exactly one unstable pair of complex conjugate eigenvalues, and linear instability of $\mathbf{w}_e$ gives rise to a laminar time-periodic solution in which alternating vortices are shed aft of the airfoil. Here, we consider the case $Re = 1000$ and $\alpha = 10°$, for which the base flow (figure 6a) is linearly unstable and the long-time solution (in the absence of control) is a limit cycle (figure 6b). Consistent with previous work [32], an Arnoldi calculation (figure 6c) shows that there is a single pair of unstable eigenvalues ($\omega = 0.4892 \pm 4.7028\mathrm{i}$) for the values of Re and α considered. We note that the real part of the unstable pair of eigenvalues is one order of magnitude larger than that for flow past a cylinder (for which the most unstable pair of eigenvalues is found to be $\omega = 0.0186 \pm 0.778\mathrm{i}$).

We first verify that the original approach by Blanchard et al. [15] is capable of suppressing growth of small-amplitude perturbations around $\mathbf{w}_e$. Since $\dim(\mathcal{E}_u) = 2$, we expect that the control law (14) with two (but no fewer) OTD modes should be able to prevent development of instability. The main flow is initialized on $\mathbf{w}_e$, to which is superimposed a small asymmetric inlet perturbation in the form

$$\mathbf{w}_{inlet}(y, t = 0) = (1 + 0.0001y)\mathbf{e}_x. \tag{26}$$
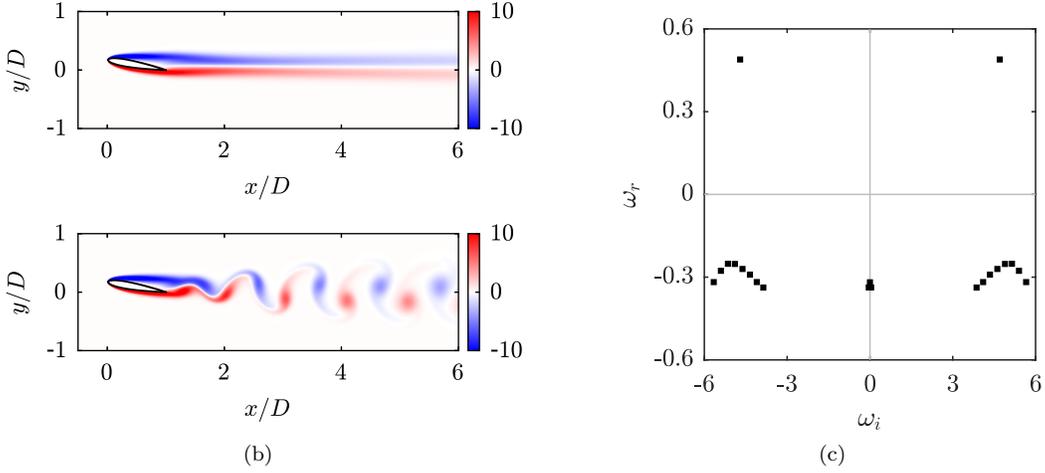
FIG. 6. For flow past a NACA 0012 airfoil with $\alpha = 10°$ and $Re = 1000$, (a) spanwise vorticity distribution of the steady solution, (b) snapshot of the spanwise vorticity distribution of the solution on the limit cycle at an instant for which C_L is maximum, and (c) 21 most unstable eigenvalues of the linear operator $\mathbf{L}_e$ visualized in the complex plane.

For the initial conditions of the OTD modes, we apply Gram–Schmidt orthonormalization to the subspace $\{\sin(my)\mathbf{e}_x + \cos(mx)\mathbf{e}_y\}_{m=1}^r$. The control is active for all $t \geq 0$. Figure 7a shows time series for $|C_L - C_{L,e}|$ (where $C_{L,e}$ is the value of the lift coefficient for $\mathbf{w}_e$) for $r = 1$ and 2, and $\zeta = 0.1$. Clearly, OTD control with $r = 2$ successfully suppresses asymptotic growth of the imposed perturbation, while OTD control with $r = 1$ does not.

Next, we consider a trajectory that evolves on the limit cycle, and use OTD control to take it out and steer it toward $\mathbf{w}_e$. Computations are performed with $r = 2$ (the smallest value of r required for stabilization of $\mathbf{w}_e$), and the modified control law (25) to avoid temporal discontinuities in the control force. We consider three values of the damping coefficient ($\zeta = 1.8$, 2.4 and 3.2). The main flow initially coincides with a state of maximum lift on the limit cycle (figure 6b). Initial conditions for the OTD modes are specified as above. The control is activated at $t = 100$ and remains active for the rest of the calculation. For the three values of ζ considered, figure 7b shows that activation of the control leads to rapid stabilization of $\mathbf{w}_e$. The time elapsed between activation of the control and beginning of the final approach to $\mathbf{w}_e$ is shorter for larger values of ζ. The rate at which final approach to $\mathbf{w}_e$ takes place is essentially independent of ζ, suggesting that the values of ζ considered are sufficiently large that the rate of approach is dictated by the least stable eigendirection on which the control does not act.
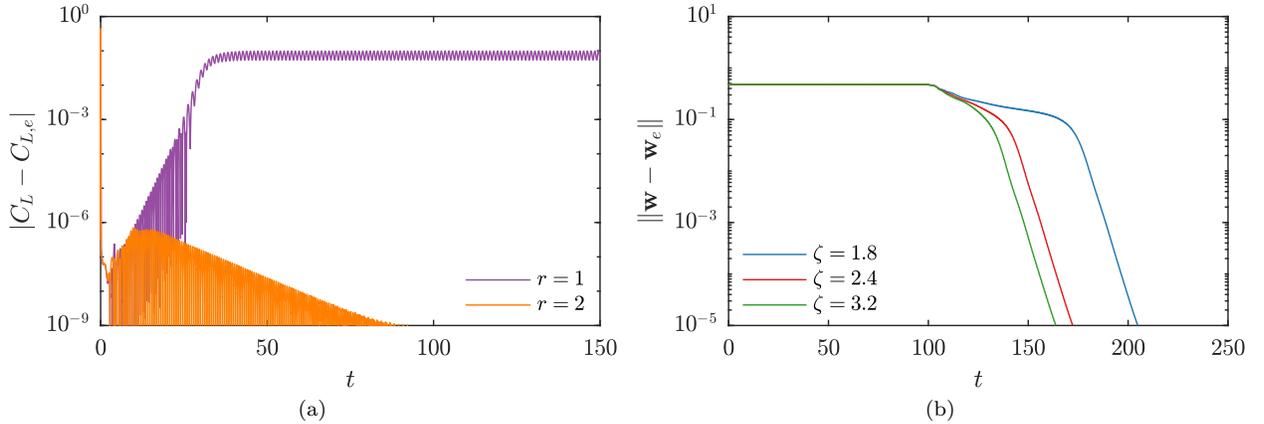
FIG. 7. For flow past a NACA 0012 airfoil with $\alpha = 10°$ and $Re = 1000$, (a) time series of $|C_L - C_{L,e}|$ for trajectories subject to infinitesimal asymmetric inlet perturbation (26) with OTD control law (14) and $\zeta = 0.1$, and (b) time series of $\|\mathbf{w} - \mathbf{w}_e\|$ for trajectories initialized on the limit cycle subject to OTD control law (25) with $r = 2$ and $\zeta = 1.8$, 2.4 and 3.2. In (a), OTD control is active for all $t \geq 0$. In (b), OTD control is idle in the interval $0 \leq t < 100$ and active for $t \geq 100$.

For $\zeta = 1.8$, inspection of the vorticity distribution of $\mathbf{f}_{c,all}$ reveals that no temporal discontinuities are present (cf. movie 3 [30]). We also note that, interestingly, although the control acts as a body force on the entire computational domain, it appears to "work its way downstream", in that stabilization and symmetrization of the wake first occurs

in the near field, before propagating to the far field. As the solution in the near field becomes more symmetric, the vorticity distribution of $\mathbf{f}_{c,all}$ evolves accordingly. For example, figure 8b shows that at $t = 120$ there is a clear difference between the vorticity distribution of $\mathbf{f}_{c,all}$ immediately aft of the airfoil (the vortices arrange themselves in a way that resembles the vorticity distribution of the unstable eigenvectors of $\mathbf{L}_e$), and that in the far field, which appears considerably less organized, and reflects the strongly asymmetric and unsteady nature of the flow in that region of the domain (cf. figure 8a). This effect is more pronounced for this geometry at this Re value than it was in the flow past a cylinder at $Re = 50$ discussed in §III B.

(a)

(b)
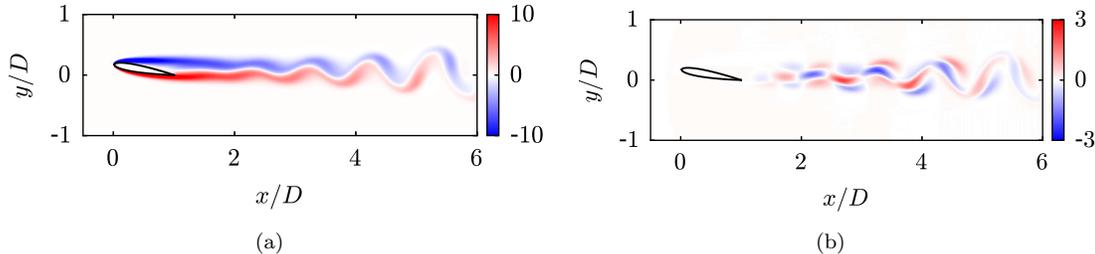
FIG. 8. For flow past a NACA 0012 airfoil with $\alpha = 10°$ and $Re = 1000$ subject to OTD control (25) with $r = 2$ and $\zeta = 1.8$, spanwise vorticity distributions of (a) the solution $\mathbf{w}$, and (b) the control force $\mathbf{f}_{c,all}$ at $t = 120$ (cf. figure 7b).

The input energy E_c required for stabilization is found to be 0.293, 0.184 and 0.163 for $\zeta = 1.8$, 2.4 and 3.2, respectively. That larger values of ζ require less energy might seem counterintuitive, but the reason is quite simple. Figure 7b shows that controller activation is followed by an interval during which $\|\mathbf{w} - \mathbf{w}_e\|$ decreases non-linearly. The duration of this interval is larger for smaller values of ζ, and ends approximately when $\|\mathbf{w} - \mathbf{w}_e\|$ falls below 0.1 (figure 7b). At that time, $\mathbf{w}$ has been brought sufficiently close to $\mathbf{w}_e$, and $\|\mathbf{w} - \mathbf{w}_e\|$ begins to decrease linearly. The bulk of the effort is done in the interval of nonlinear decay of $\|\mathbf{w} - \mathbf{w}_e\|$, as this interval corresponds to the controller pulling the trajectory out of the limit cycle. That this interval is shorter for larger values of ζ compensates for the fact that large ζ in principle increases the cost of the control.

D. Kolmogorov flow

We now consider Kolmogorov flow on the torus $\Omega = [0, 2\pi]^2$. The flow obeys the incompressible Navier–Stokes equations with sinusoidal forcing, written in dimensionless form as

$$\partial_t \mathbf{w} + \mathbf{w} \cdot \nabla \mathbf{w} = -\nabla p + \frac{1}{Re}\nabla^2 \mathbf{w} + \sin(k_f y)\mathbf{e}_x, \tag{27a}$$

$$\nabla \cdot \mathbf{w} = 0, \tag{27b}$$

where k_f is a positive integer, and the Reynolds number Re is the inverse of a dimensionless fluid viscosity ν. The OTD equations are identical to (20a,b), with $\mathbf{L}_{ns}$ given by (22). The main flow and the OTD modes satisfy periodic boundary conditions. The computational solution is effected using `nek5000` with a mesh composed of 256 elements (16 elements in each direction), polynomial order $N = 7$, and time-step size $\Delta t = 10^{-3}$.

The Kolmogorov flow admits a laminar solution,

$$\mathbf{w}_e = \frac{Re}{k_f^2}\sin(k_f y)\mathbf{e}_x, \tag{28}$$

which is asymptotically stable for forcing wave number $k_f = 1$ and any value of Re [33]. For $k_f > 1$ and large enough Re values, the laminar solution $\mathbf{w}_e$ is unstable, and the long-time solution is chaotic [34, 35]. Other invariant solutions besides (28) are known to exist for this flow. For $k_f = 4$ and $Re = 40$, Farazmand [36] reported no fewer than 16 different steady (unstable) solutions, with $\dim \mathcal{E}_u$ ranging from 5 to 38. In [15], Blanchard et al. were able to stabilize the laminar solution (28) (for which $\dim \mathcal{E}_u = 38$) in the limit of small perturbations by applying the control law (14) with 38 OTD modes.

In the wake of Blanchard et al. [15], we consider parameters $k_f = 4$ and $Re = 40$ for which (28) is linearly unstable, and the long-time solution is chaotic. Here, we use OTD control to annihilate the chaotic attractor and steer the trajectory to the fixed point (28). We note that the temporal regularity of the long-time (chaotic) attractor is lower than in the previous examples considered. (The long-time attractor was a fixed point in §III A, and a time-periodic orbit in §§III B and III C.) The main flow is initialized on the chaotic attractor (cf. figure 9a). To initialize the OTD

modes, we apply Gram–Schmidt orthonormalization to the subspace $\{\cos(mx)\sin(my)\mathbf{e}_x - \sin(mx)\cos(my)\mathbf{e}_y\}_{m=1}^r$. The OTD modes thus satisfy the incompressibility constraint and the periodic boundary conditions at $t = 0$. For the first 50 convective time units, the control is idle, and the trajectory wanders on the chaotic attractor. The control is activated at $t = 50$, and remains active for the rest of the computation.

Figure 9b shows time series for the energy dissipation

$$E_d(t) = \frac{1}{Re|\Omega|}\int_\Omega |\nabla \mathbf{w}|^2 \mathrm{d}\Omega \tag{29}$$

for the uncontrolled case ($r = 0$), and three controlled cases with various values of r and control law (14). We first note that in the absence of control, the trajectory remains on the chaotic attractor and never approaches the laminar solution $\mathbf{w}_e$ (for which $E_d = 1.25$). We also note that for $r = 38$, the smallest value for which stabilization of $\mathbf{w}_e$ is possible in the limit of infinitesimal perturbations, OTD control is not able to annihilate the chaotic attractor. (The calculation was terminated at $t = 1500$ to give credibility to this claim.) This is in stark contrast with the previous examples in §§III A, III B and III C, in which choosing $r = \max(\dim\mathcal{E}_u, \dim\mathcal{E}_u^s)$ was sufficient to guarantee success of the control strategy, notwithstanding that this criterion was based on the assumption that disturbance amplitude remained small. Kolmogorov flow is thus the first example that we encounter in which r must be strictly greater than $\max(\dim\mathcal{E}_u, \dim\mathcal{E}_u^s)$ for OTD control to annihilate the attractor. As discussed in §II B, this is a consequence of the fact that in the chaotic regime, $\|\mathbf{w} - \mathbf{w}_e\|$ is not small: the number of unstable directions on the attractor, or along the path from the attractor to the target, may well exceed the number of unstable directions close to $\mathbf{w}_e$. For stabilization to be possible, the controller must act on all unstable directions, from the moment the trajectory leaves the attractor to the final approach to the target. So it is not surprising that in some cases, we need a larger number of OTD modes than that prescribed by linearized theory. But, as noted in §III.B, we cannot afford to use fewer modes than $\max(\dim\mathcal{E}_u, \dim\mathcal{E}_u^s)$, because otherwise stabilization close to $\mathbf{w}_e$ would not be possible.
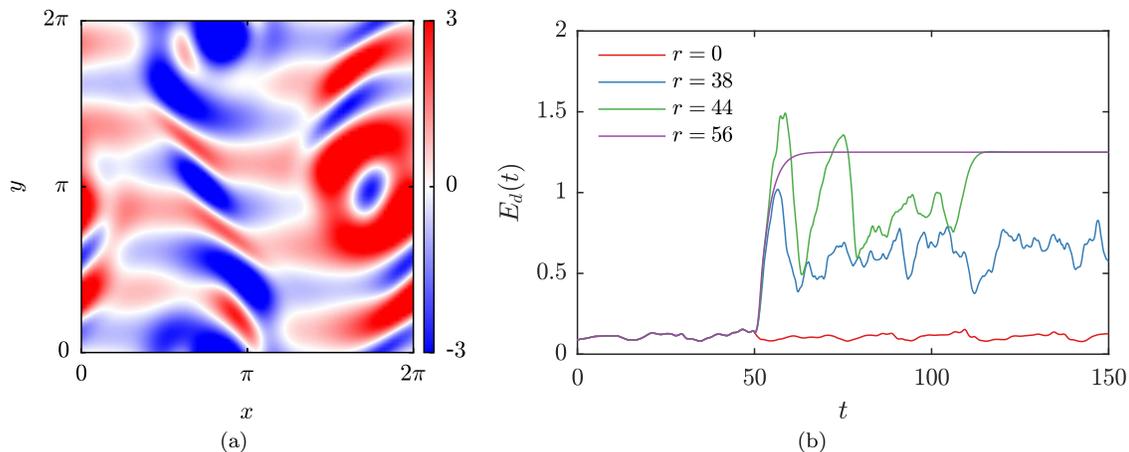
FIG. 9. For Kolmogorov flow with $Re = 40$ and $k_f = 4$, (a) spanwise vorticity distribution of the initial condition used in the computations, and (b) energy dissipation for trajectories with OTD control (with $\zeta = 0.1$), and without control. Control is idle in the interval $0 \le t < 50$ and active for $t \ge 50$.

To determine the critical value of r for which destruction of the chaotic attractor by OTD control is possible, we proceed by bisection. But first, we must note that because the original control law (14) is based on linearization assumptions, there is no guarantee that there exists a low-dimensional OTD control strategy capable of stabilizing $\mathbf{w}_e$ for large-amplitude disturbances. In fact, when linearization does not hold, the only available bound on the critical OTD subspace dimension is $\max(\dim\mathcal{E}_u, \dim\mathcal{E}_u^s) \le r \le d$, where d is the dimension of the phase space. So our hope is that there exists a value of r not too greater than $\max(\dim\mathcal{E}_u, \dim\mathcal{E}_u^s)$ such that (14) is efficient, although nothing guarantees it *a priori*. The results are shown in figure 9b. We find that OTD control with $r = 56$ is able to stabilize $\mathbf{w}_e$. A refined search shows that no fewer than 44 OTD modes should be included in order to destroy the chaotic attractor.

For $r = 44$, movie 4 [30] shows time series for E_d cued to the vorticity distributions of $\mathbf{w}$ and $\mathbf{f}_c$. The latter exhibits large-scale coherent structures in the transient interval during which the trajectory is pulled out of the chaotic attractor (from $t = 50$ to about 115). At longer times (after about $t = 115$), the trajectory approaches the fixed point, and the OTD subspace aligns with the most unstable eigenspace of $\mathbf{L}_e$. When $\mathbf{w}$ is infinitesimally close to $\mathbf{w}_e$, only 38 of the 44 OTD directions are acted upon by the control. For $r = 56$, movie 5 [30] and figure 9b

show that $\mathbf{w}$ approaches $\mathbf{w}_e$ much more rapidly than for $r = 44$, which suggests that including more OTD modes in the controller can prevent "overshoot" of the solution and accelerate stabilization. Finally, we note that the input energy E_c required by the control is two orders of magnitude larger for $r = 44$ (1106.8) than for $r = 56$ (78.68). This discrepancy has to do with the fact that stabilization is achieved much more rapidly in the latter case.

This completes demonstration of robustness of OTD control in situations where the trajectory initially evolves on an attractor far from the target fixed point. We found no instances in which the OTD controller had a destabilizing effect on the dynamics. We conjecture that this is because the OTD modes are computed along the trajectory, and therefore are able to adapt to situations in which the state of the system is not close to the target fixed point. The examples discussed above indeed made clear that the OTD modes "deform" as the trajectory visits various regions in the phase space, including during its journey from the unsteady attractor to the target fixed point.

IV.   STABILIZATION OF UNSTEADY FLOWS BY SPATIALLY LOCALIZED OTD CONTROL

The results presented in §III were generated with a control strategy in which it was assumed that the control had knowledge of, and could act on, every state variable of the system. In other words, the system was assumed fully observable and fully controllable. As discussed §I, this approach has limited applicability from the standpoint of conducting experiments, since in practice the range and number of sensors and actuators is limited by the apparatus. In this section, we attempt to address this issue, and propose a modified OTD control strategy in which the range of action of the controller is restricted to a small portion of the physical domain, and the control law (including the OTD modes) is computed solely based on the knowledge of the primitive variables in that subdomain.

A.   Formulation of a spatially localized OTD control law

To formulate a practical OTD control law, we assume that range of actuation and access to flow data are limited to a convex subdomain $\bar{\Omega}$ of the physical domain Ω in which experiments or computations are performed. This assumption immediately excludes a "naive" control strategy in which the control force $\mathbf{f}_c$ would be computed on the entire domain Ω (as in §III), and on which a mask would be applied that sets the value of $\mathbf{f}_c$ to zero in $\Omega \setminus \bar{\Omega}$, and leaves it unaltered otherwise. We further assume that the state $\bar{\mathbf{z}}$ of the system in $\bar{\Omega}$ is known with exactitude. The question then is to find an appropriate formulation for computing the OTD modes in $\bar{\Omega}$, given sole knowledge of the state in $\bar{\Omega}$.

1.   Computation of localized OTD modes

To help us with the formulation, we make a brief incursion in the infinite-dimensional setting. We consider a generic dynamical system whose evolution obeys $\partial_t z = \mathscr{F}(z)$, where z belongs to an appropriate function space $\mathcal{X}$ defined in $\Omega \times \mathbb{R}^+$, and $\mathscr{F}$ is a nonlinear differential operator. Infinitesimal perturbations about a trajectory obey the variational equations $\partial_t v = \mathscr{L}(z; v)$, where $v \in \mathcal{X}$ and $\mathscr{L}(z; v) = \mathrm{d}\mathscr{F}(z; v)$ is the Gâteaux derivative of $\mathscr{F}$ evaluated at z along the direction v. The lower triangular OTD system can be written as

$$\partial_t u_i = \mathscr{L}(z; u_i) - \langle \mathscr{L}(z; u_i), u_i \rangle u_i - \sum_{k=1}^{i-1} \left[\langle \mathscr{L}(z; u_i), u_k \rangle + \langle \mathscr{L}(z; u_k), u_i \rangle \right] u_k, \quad 1 \le i \le r, \tag{30}$$

where it is understood that each u_i belongs to $\mathcal{X}$, and therefore is defined in $\Omega \times \mathbb{R}^+$. The OTD equations obtain at every point $x \in \Omega$, so *a fortiori* at every $x \in \bar{\Omega}$. Therefore, we may use (30) to compute the OTD modes in $\bar{\Omega}$. The question then arises as to what boundary conditions should be specified on $\partial \bar{\Omega}$ for the modes. A natural answer is to use homogeneous Dirichlet boundary conditions. This choice is appropriate for the following reason. Here, we have restricted ourselves to controlling the flow in $\bar{\Omega}$ only, so the control force must vanish outside of the control domain. But we recall from §II B that dynamical consistency of the order reduction demands that the control force belong to the OTD subspace. Hence, use of homogeneous Dirichlet boundary conditions for the OTD modes guarantees that the resulting control force $\mathbf{f}_c$ is continuous across $\partial \bar{\Omega}$.

Use of homogeneous Dirichlet boundary conditions on $\partial \bar{\Omega}$ for the OTD modes is consistent only if we recover the original OTD modes (i.e., those computed in the full domain Ω) in the limit when $\bar{\Omega} \to \Omega$. For open flows of infinite extent, the far-field velocity components for the base flow are specified as inhomogeneous Dirichlet boundary conditions (e.g., equation (19b)). In that case, infinitesimal perturbations about the base flow (and likewise, OTD

modes) *must* satisfy homogeneous Dirichlet boundary conditions in the far field (e.g., equation (21b)), so there is no incompatibility of the boundary conditions as $\bar{\Omega} \to \Omega$. The issue arises when the flow domain has finite extent, e.g., in physically bounded flows, and in any *computation* of open flows. In the latter case, there is no accepted answer to the question of what boundary conditions are appropriate for the linearized dynamics. The only related investigation of which we are aware was done by Peplinski et al. [37]. For flow past a circular cylinder at $Re = 50$, and for other open flows, including Poiseuille flow and jet in cross-flow, Peplinski et al. [37] showed that the effect of boundary conditions on the most unstable eigenvalues of the linearized operator (i.e., those responsible for linear instability of the base flow) is minuscule, and that only the high-frequency, highly damped modes appear to be significantly affected. Heuristically, this is because the stronger instabilities should not be affected by the flow conditions in the far field, as long as the computational domain is large enough.

Based on this discussion, we decide to specify homogeneous Dirichlet boundary conditions for the OTD equation regardless of the domain in which the OTD modes are computed. The spatially discretized OTD equation retains a form similar to (6), but now $\mathbf{U}$ and $\mathbf{L}$ are computed in a subdomain $\bar{\Omega}$ with homogeneous Dirichlet boundary conditions on $\partial\bar{\Omega}$. We will denote these quantities by $\bar{\mathbf{U}} \in \mathbb{R}^{m \times r}$ and $\bar{\mathbf{L}} \in \mathbb{R}^{m \times m}$, respectively, where m is the number of degrees of freedom associated with $\bar{\Omega}$ ($m = d$ when $\bar{\Omega} = \Omega$). (We note that the OTD modes computed in $\bar{\Omega}$ satisfy the orthonormality condition in $\bar{\Omega}$.) This allows us to formulate a new control law,

$$\bar{\mathbf{f}}_{c,sub} = \bar{\mathbf{U}}\bar{\mathbf{Q}}\text{diag}[-(\bar{\lambda}_i + \zeta)\mathscr{H}(\bar{\lambda}_i)]\bar{\mathbf{Q}}^\mathsf{T}\bar{\mathbf{U}}^\mathsf{T}\mathbf{R}(\mathbf{z} - \mathbf{z}_e), \tag{31}$$

where $\bar{\mathbf{Q}}$ and $\{\bar{\lambda}_i\}_{i=1}^r$ are the eigenvectors and eigenvalues of $(\bar{\mathbf{L}}_r + \bar{\mathbf{L}}_r^\mathsf{T})/2$, respectively, and $\mathbf{R} \in \mathbb{R}^{m \times d}$ is a rank-m restriction matrix that excises from the full state $\mathbf{z}$ those degrees of freedom associated with $\Omega \setminus \bar{\Omega}$, and retains those in the interior of $\bar{\Omega}$. The presence of the restriction operator left-multiplying the deviation $\mathbf{z} - \mathbf{z}_e$ reflects the fact that only part of the state is accessible. To facilitate application of the control force to the governing equations (which are defined in Ω), we pre-multiply $\bar{\mathbf{f}}_{c,sub}$ by the prolongation matrix $\mathbf{R}^\mathsf{T}$, which gives

$$\mathbf{f}_{c,sub} = \mathbf{R}^\mathsf{T}\bar{\mathbf{U}}\bar{\mathbf{Q}}\text{diag}[-(\bar{\lambda}_i + \zeta)\mathscr{H}(\bar{\lambda}_i)]\bar{\mathbf{Q}}^\mathsf{T}\bar{\mathbf{U}}^\mathsf{T}\mathbf{R}(\mathbf{z} - \mathbf{z}_e). \tag{32}$$

The modified control force (32) is defined in Ω, by construction vanishes outside of $\bar{\Omega}$, and is C^0-continuous across $\partial\bar{\Omega}$.

We note that in a realistic (experimental) set-up, actuation is typically achieved using boundary control (e.g., blowing and suction on the surface of a bluff body [38] or near the upstream edge of a cavity [39]). However, use of a localized body force such as (32) is far from irrelevant. First, as others have noted [40], this approach facilitates analysis and evaluation of control performance. Second, it often is the case that boundary actuation can be represented as a Galerkin superposition of actuation modes that mimic the effect of a body force [41, 42]. Third, this approach has encountered a great deal of success in a range of flow control problems, including flow past a cylinder [43] and an airfoil [44], and synthetic jets [45]. We also note that other localized control strategies have been found quite successful, including use of a splitter plate to manipulate the flow immediately behind a bluff body in order to mitigate wake separation [46, 47]. The addition of a splitter plate aft of a bluff body can be thought of as enforcement of a discontinuity in the primitive variables along the span of the splitter plate. This is in contrast to the proposed localized OTD control strategy, in which the actuation produces no artificial discontinuity in the flow field.

2. *Selection of control domain*

We now have a recipe to compute the OTD modes in a localized domain based on which we were able to formulate a localized control law. We must now address the question of how to select the size and location of the control subdomain. We first note that information related to transient instabilities is contained in the full-order linearized operator $\mathbf{L}$ (which is defined globally in Ω). For hyperbolic fixed points, all this information is retained upon OTD reduction, provided that the dimension of the OTD subspace is large enough [15]. However, this no longer holds when the OTD modes are computed in a subdomain. So to evaluate the extent to which restriction of Ω to a smaller $\bar{\Omega}$ affects the instability properties of the linearized operator, we consider a measure of instability based on the OTD modes.

We assume for the moment that the OTD modes are computed in the full domain Ω. We let

$$V_k(t) = \|\wedge_{j=1}^k \mathbf{u}_j(t)\| \tag{33}$$

be the volume of the k-dimensional parallelepipeds spanned by the first k OTD modes. Defining

$$\nu_j(t) = \langle \mathbf{L}\mathbf{u}_j, \mathbf{u}_j \rangle \tag{34}$$

as the jth *instantaneous OTD eigenvalue*, we note that the rate of change of $V_k(t)$, which characterizes the instantaneous growth or decay of the reference volume $V_k(t)$ at time t, satisfies

$$\frac{\mathrm{d}\ln V_k(t)}{\mathrm{d}t} = \sum_{j=1}^{k} \nu_j(t). \tag{35}$$

As discussed in Blanchard & Sapsis [20], the long-time average of (35) coincides with the k-dimensional infinite-horizon Lyapunov exponent

$$\mu^{(k)} = \lim_{t\to\infty} \frac{1}{t-t_0}\ln V_k(t), \tag{36}$$

while the one-dimensional infinite-horizon Lyapunov exponent μ_j associated with the jth "edge" of the parallelepiped in (33) is nothing more than

$$\mu_j = \lim_{t\to\infty} \frac{1}{t-t_0}\int_{t_0}^{t} \nu_j(\tau)\mathrm{d}\tau. \tag{37}$$

This suggests that the instantaneous OTD eigenvalues ν_j, or equivalently, their long-time averages μ_j, may serve as indicators to determine how much information associated with instabilities the OTD subspace captures. Interestingly, for $k = d$ (the dimension of the phase space), we have that

$$\frac{\mathrm{d}\ln V_d}{\mathrm{d}t} = \nabla \cdot \mathbf{F}, \tag{38}$$

which is simply the divergence of the vector field $\mathbf{F}$. Quite obviously, when the operator $\mathbf{L}$ is steady (e.g., evaluated at a fixed point), the volume V_k grows like the k most unstable eigenvalues of the operator because the OTD subspace coincides with the most unstable eigenspace $\mathcal{E}_u$.

The instantaneous OTD eigenvalues $\{\nu_j\}_{j=1}^{r}$ depend only on the OTD modes and the linearized operator, and are therefore oblivious to whether the OTD modes are computed in the original domain Ω, or a localized domain $\bar{\Omega}$. So we may define the jth *localized* instantaneous OTD eigenvalue as

$$\bar{\nu}_j(t) = \langle \bar{\mathbf{L}}\bar{\mathbf{u}}_j, \bar{\mathbf{u}}_j \rangle, \tag{39}$$

where $\bar{\mathbf{u}}_j$ is the jth column of $\bar{\mathbf{U}}$, as well as its long-time average, which we denote by $\bar{\mu}_j$. We note that μ_j and $\bar{\mu}_j$ are real numbers, so they may be compared with one another. In particular, we have that $\bar{\mu}_j \to \mu_j$ as $\bar{\Omega} \to \Omega$. Moreover, there is every reason to believe that for subdomains $\bar{\Omega}$ smaller than Ω, the localized OTD eigenvalue $\bar{\mu}_j$ will differ from its "global" counterpart μ_j by some measurable amount. This observation suggests that the difference between $\bar{\mu}_j$ and μ_j may serve as an indicator for how much information related to instability the OTD modes are able to capture when computed in a smaller domain $\bar{\Omega}$. For example, in flow past a cylinder, we expect $\bar{\mu}_j$ to greatly differ from μ_j if $\bar{\Omega}$ is selected as some region in the far field where the flow is uniform, much more than if $\bar{\Omega}$ includes a substantial fraction of the near field where the wake instability develops and the vortex shedding appears. In the following examples, we provide numerical evidence that the $\bar{\mu}_j$'s (more precisely, the leading exponent $\bar{\mu}_1$) are indeed good indicators for selection of the control domain.

B. Application to bluff-body flows

We return to the flow past a circular cylinder at $Re = 50$ considered in §III B. We begin by verifying the claim made by Peplinski et al. [37] that the most unstable eigenvalues of $\mathbf{L}_e$ are virtually unaffected by a change in the far-field computational boundary conditions on $\partial\Omega$. For the mesh used in §III B, we compute the spectrum of $\mathbf{L}_e$ by an Arnoldi algorithm for two sets of far-field boundary conditions. The first set corresponds to the original boundary conditions that were used in §III B, i.e., homogeneous Dirichlet boundary conditions at the inlet, stress-free boundary condition at the outlet, and symmetry boundary conditions on the sidewalls. The second set corresponds to homogeneous Dirichlet boundary conditions specified at the inlet, outlet and on the sidewalls. For these two sets of boundary conditions, a no-slip boundary condition is specified on the cylinder surface. Figure 10a shows that consistent with Peplinski et al. [37], the two unstable eigenvalues responsible for linear instability of $\mathbf{w}_e$ are largely unaffected by a change in the far-field boundary conditions. This is important because it is those eigenvalues that OTD control asymptotically targets. Figure 10a also shows that the stable eigenvalues are much more sensitive to boundary conditions. Specifically, the
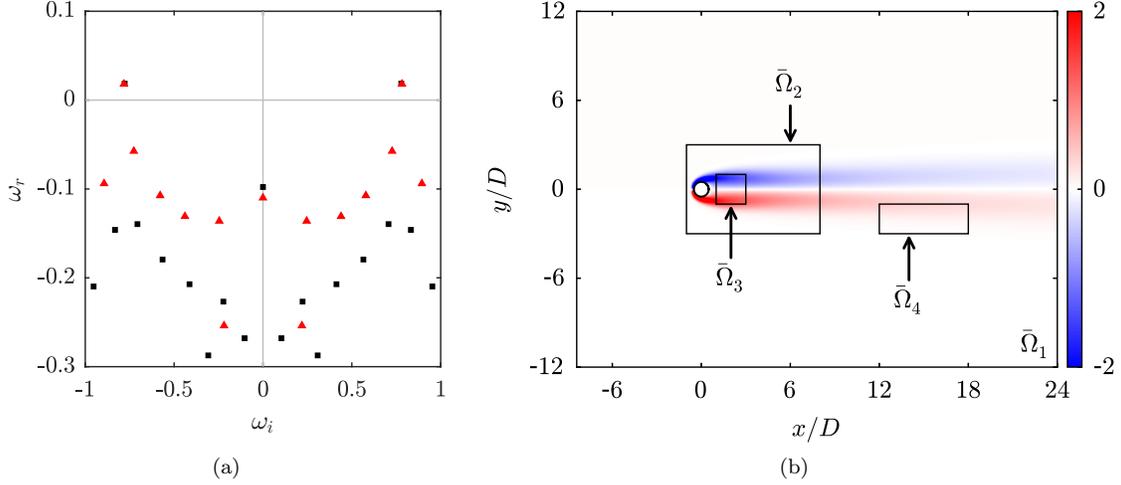
FIG. 10. For flow past a cylinder at $Re = 50$, (a) spectrum of $\mathbf{L}_e$ computed with inflow-outflow-symmetry boundary conditions (black squares) and homogeneous Dirichlet boundary conditions (red triangles), and (b) location of control subdomains $\bar{\Omega}_1$ to $\bar{\Omega}_4$ with the spanwise vorticity distribution of $\mathbf{w}_e$ shown in the background.

real parts of the stable eigenvalues are larger when homogeneous Dirichlet boundary conditions are specified on $\partial\Omega$. Fortunately, no spurious unstable eigenvalues have appeared, so this discrepancy (which was also noted by Peplinski et al. [37]) has no consequence for our control strategy.

We proceed to investigate what "fraction" of instability the OTD modes are able to capture when they are computed in a localized domain $\bar{\Omega}$. We compute long-time averages of the instantaneous OTD eigenvalues for an 8-dimensional OTD subspace and the four subdomains shown in figure 10b. The first ($\bar{\Omega}_1$) coincides with Ω, and therefore serves as a sanity check, as the OTD eigenvalues in Ω can be directly compared against those computed by the Arnoldi algorithm. The second ($\bar{\Omega}_2 = \{(x,y) : x \in [-1,8],\, y \in [-3,3]\}$) corresponds to a rectangular domain that contains the cylinder and part of the near wake. The third ($\bar{\Omega}_3 = \{(x,y) : x \in [1,3],\, y \in [-1,1]\}$) corresponds to a square domain that extends over a smaller area in the near wake, immediately behind the cylinder. The fourth ($\bar{\Omega}_4 = \{(x,y) : x \in [12,18],\, y \in [-3,-1]\}$) corresponds to a rectangular domain located further downstream where the flow is nearly uniform.

Table I lists the long-time averages $\bar{\mu}_j$ of the instantaneous OTD eigenvalues for the four subdomains introduced above, along with the real part μ_j of the eight most unstable eigenvalues of $\mathbf{L}_e$ computed by an Arnoldi algorithm (the red triangles in figure 10a). For a fair comparison, we use the steady linearized operator $\mathbf{L}_e$ in the computation of the OTD eigenvalues. Table I shows that for $\bar{\Omega}_1$, the OTD eigenvalues $\bar{\mu}_j$ agree with the results of the Arnoldi calculation to within 3%. For $\bar{\Omega}_2$, the leading pair of eigenvalues $\{\bar{\mu}_{1,\bar{\Omega}_2}, \bar{\mu}_{2,\bar{\Omega}_2}\}$ is close to $\{\mu_1, \mu_2\}$, but the other eigenvalues $\{\bar{\mu}_{j,\bar{\Omega}_2}\}_{j\geq 3}$ are not close to $\{\mu_j\}_{j\geq 3}$. For $\bar{\Omega}_3$ and $\bar{\Omega}_4$, the eigenvalues are all negative, with $\bar{\mu}_{1,\bar{\Omega}_3}$ slightly closer to μ_1 than $\bar{\mu}_{1,\bar{\Omega}_4}$.

j	μ_j	$\bar{\mu}_{j,\bar{\Omega}_1}$	$\bar{\mu}_{j,\bar{\Omega}_2}$	$\bar{\mu}_{j,\bar{\Omega}_3}$	$\bar{\mu}_{j,\bar{\Omega}_4}$
1	0.0181	0.0177	0.0157	-0.4615	-0.5127
2	0.0181	0.0177	0.0157	-0.4615	-0.5385
3	-0.0574	-0.0591	-0.1287	-0.8498	-0.5385
4	-0.0574	-0.0591	-0.1287	-0.8498	-0.5530
5	-0.0939	-0.0940	-0.3765	-0.8668	-0.5530
6	-0.0939	-0.0940	-0.3765	-1.1903	-0.6139
7	-0.1073	-0.1084	-0.4083	-1.1903	-0.6139
8	-0.1073	-0.1084	-0.4083	-1.1903	-0.6432

TABLE I. For flow past a cylinder at $Re = 50$, real part of the eight most unstable eigenvalues μ_j computed by an Arnoldi method, compared to the leading eight time-averaged OTD eigenvalues $\bar{\mu}_{j,\bar{\Omega}_k}$ computed in control subdomain $\bar{\Omega}_k$ (cf. figure 10b) with $r = 8$.

To interpret the results in table I, we apply OTD control to the subdomains $\{\bar{\Omega}_k\}_{k=1}^4$. In recognition of the fact that the long-time OTD eigenvalues for $\bar{\Omega}_3$ and $\bar{\Omega}_4$ are all negative, we substitute $\mathrm{diag}[-(\bar{\lambda}_i + \zeta)\mathscr{H}(\bar{\lambda}_i)]$ for $\mathrm{diag}(-\zeta)$

in (32), so that damping is applied to each of the OTD directions. If we were to use (32) for $\bar{\Omega}_3$ and $\bar{\Omega}_4$, the controller would be idle at long times because all the $\bar{\mu}_j$'s would be negative, and stabilization would therefore be impossible. As in §III B, we assume that the trajectory initially evolves on the limit cycle and activate OTD control at $t = 100$. For $r = 8$ and $\zeta = 0.4$, figure 11a shows that the *localized* OTD controller is able to stabilize $\mathbf{w}_e$ *globally* for $\bar{\Omega}_1$, $\bar{\Omega}_2$ and $\bar{\Omega}_3$ (cf. movie 6 [30]). These are cases in which the control domain extends over flow regions that are "relevant" to the overall dynamics. By contrast, for the poorly selected domain $\bar{\Omega}_4$, OTD control fails to stabilize $\mathbf{w}_e$. For the three subdomains for which stabilization is achieved, figures 11a,b show that the approach to $\mathbf{w}_e$ is faster when the control subdomain is larger. The input energy E_c normalized by the size of the control domain is found to be 8.04×10^{-4}, 2.24×10^{-3} and 2.46×10^{-3} for $\bar{\Omega}_1$, $\bar{\Omega}_2$ and $\bar{\Omega}_3$, respectively. These numbers suggest that use of a localized controller does not necessarily lead to a reduction in power requirement, largely because the approach to $\mathbf{w}_e$ is slower for the localized controllers considered here (cf. figure 11a).

(a)　　　　　　　　　　　　　　　　　　(b)
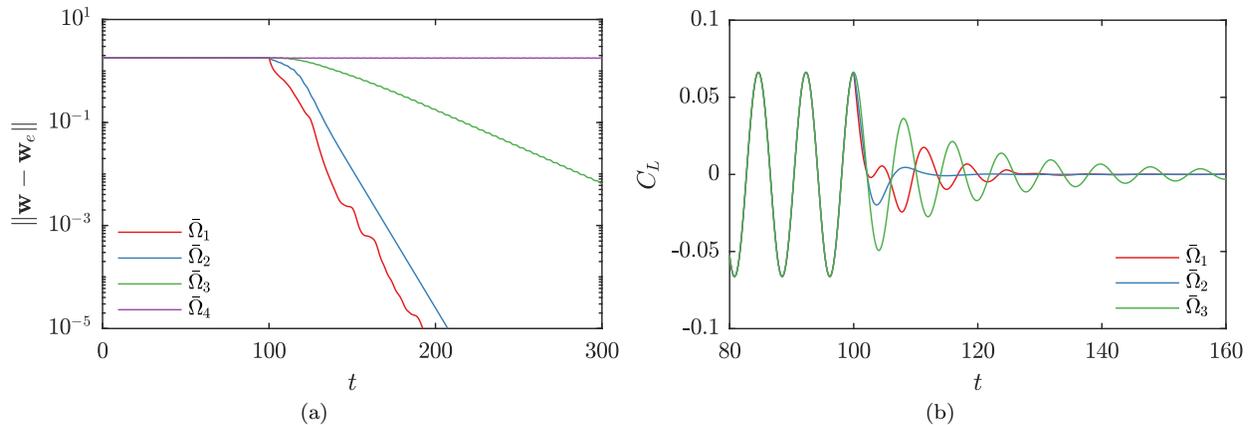
FIG. 11. For flow past a cylinder at $Re = 50$ subject to localized OTD control with $r = 8$, $\zeta = 0.4$ and the control subdomains $\bar{\Omega}_k$ shown in figure 10b, (a) time series of $\|\mathbf{w} - \mathbf{w}_e\|$, and (b) detail of the time series for C_L. Control is idle in the interval $0 \leq t < 100$ and active for $t \geq 100$.

The results in table I and figures 11a,b suggest that to achieve stabilization, the OTD control subdomain should cover a portion of the computational domain that is relevant to the instability mechanism. Here, "relevance" of a subdomain $\bar{\Omega}$ can be characterized by the leading time-averaged OTD eigenvalue $\bar{\mu}_1$ (cf. table I). The closer $\bar{\mu}_1$ is to the actual Lyapunov exponent μ_1, the more efficient the OTD controller should be. Of course, the values reported in table I suggest that a larger control subdomain is more efficient, since $\bar{\mu}_{1,\bar{\Omega}_2}$ is much closer to μ_1 than $\bar{\mu}_{1,\bar{\Omega}_3}$. However, the fact that OTD control in $\bar{\Omega}_3$ also leads to stabilization shows that this criterion is best used for comparing two candidate subdomains of *identical dimensions*, rather than to decide on the absolute "worthiness" of a subdomain.

In light of this, it is natural to ask whether a strategy can be proposed for optimally selecting the control subdomain, given a particular subdomain size. To this end, we consider a subdomain $\bar{\Omega}$ with *fixed dimensions*, and systematically study how varying the *location* of $\bar{\Omega}$ affects the leading eigenvalue $\bar{\mu}_1$. Specifically, we consider a square subdomain extending $2D$ in the streamwise and cross-stream directions (with the sidewalls parallel to the y-axis), and vary the location of its center (x_c, y_c). Here, we do not attempt to solve the full optimization problem, but rather consider 15 combinations of x_c and y_c, with x_c/D ranging from 1 to 5 in increments of 1, and y_c/D ranging from -1 to 1 in increments of 1. Figure 12 shows that, of the 15 (x_c, y_c) pairs considered, those for which the subdomain is not symmetric about the midplane (i.e., those with $y_c \neq 0$), and those for which the subdomain is located several diameters downstream of the cylinder center, are associated with smaller values of $\bar{\mu}_1$ than otherwise. The combination of x_c and y_c for which $\bar{\mu}_1$ is the largest is $(x_c, y_c) = (2D, 0)$, corresponding to a subdomain located immediately behind the cylinder rear stagnation point (this domain is actually $\bar{\Omega}_3$). For this (x_c, y_c) pair, figures 11a,b and movie 6 [30] showed that OTD control was able to stabilize $\mathbf{w}_e$. The results in figure 12 thus suggest a strategy for selecting the location of the OTD controller when the size of the control subdomain is prescribed: the optimal subdomain is the one for which $\bar{\mu}_1$ is largest. Interestingly, the optimal control subdomain for the (x_c, y_c) pairs considered in figure 12 nearly coincides with the control volume used by Tadmor et al. [40] for the same flow. These results also suggest possible connections between the optimal OTD control subdomain and flow regions in which the flow is most "receptive" or "sensitive" [10, 48, 49]. We leave exploration of this issue to future investigation.

Finally, we apply the above methodology to flow past a NACA 0012 airfoil with $\alpha = 10°$ and $Re = 1000$, and computational parameters identical to those used in §III C. We consider a square control subdomain with fixed dimensions ($0.5L_c$ in the streamwise and cross-stream directions), and 10 combinations of (x_c, y_c) for the location of its center, with x_c/L_c ranging from 1.25 to 2.25 in increments of 0.25 and y_c/L_c ranging from -0.2 to 0.05 in
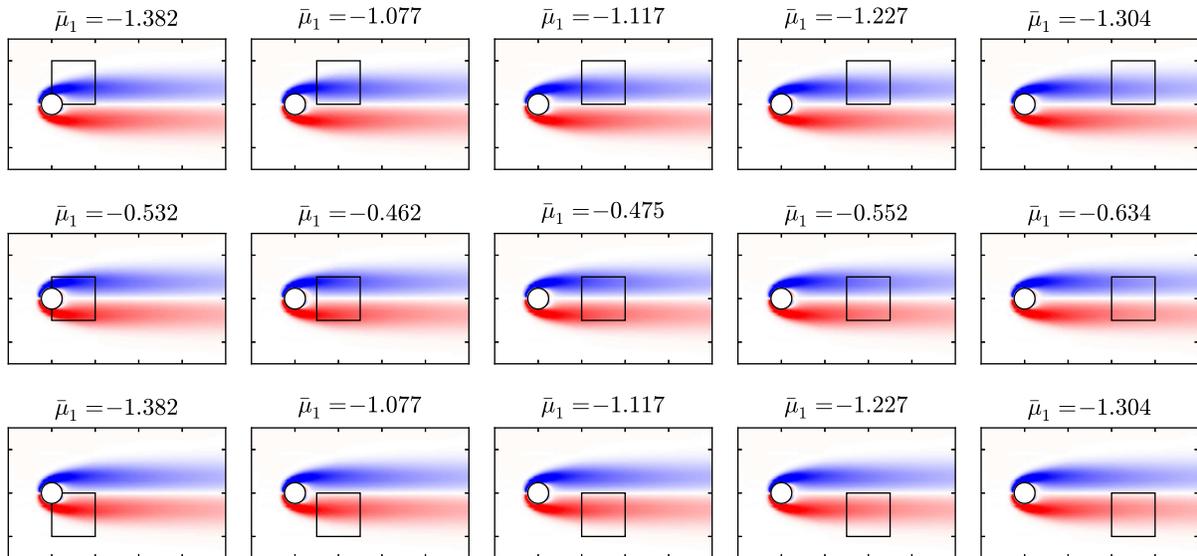
FIG. 12. For flow past a cylinder at $Re = 50$, leading time-averaged OTD eigenvalue $\bar{\mu}_1$ computed with $r = 8$ on various subdomains extending $2D$ in the streamwise and cross-stream directions (black bounding boxes). The spanwise vorticity distribution of $\mathbf{w}_e$ is shown in the background.

increments of 0.25. Figure 13 shows that the leading OTD eigenvalue $\bar{\mu}_1$ follows a similar trend as in the cylinder flow. In particular, $\bar{\mu}_1$ is larger for subdomains located immediately behind the airfoil and encompassing the two recirculation bubbles. For the optimal (x_c, y_c) pair considered in figure 13 ($x_c = 1.5L_c$ and $y_c = 0.05L_c$), figure 14 shows that OTD control stabilizes the flow with no difficulty, at a cost of $E_c = 0.716$. When normalized by the size of the control subdomain, this cost becomes 2.864. (For a controller with the same parameters but acting in the entire domain, the normalized cost is found to be 2.56×10^{-3}.)
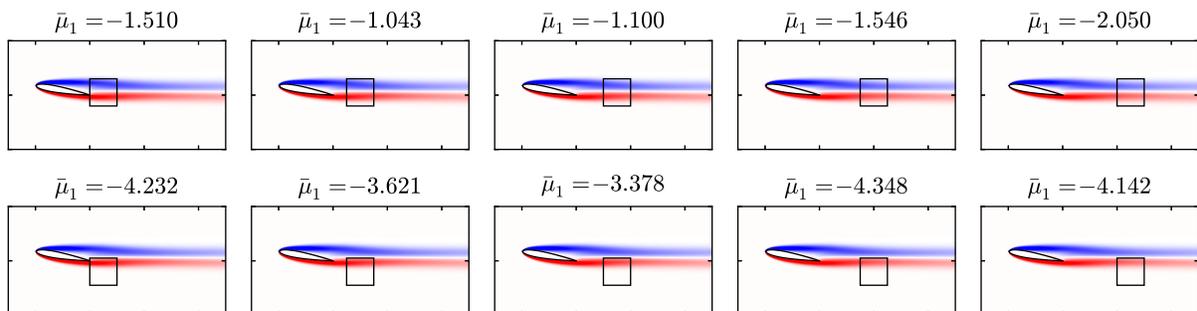
FIG. 13. For flow past a NACA 0012 airfoil with $\alpha = 10°$ at $Re = 1000$, leading time-averaged OTD eigenvalue $\bar{\mu}_1$ computed with $r = 8$ on various subdomains extending $0.5L_c$ in the streamwise and cross-stream directions (black bounding boxes). The spanwise vorticity distribution of $\mathbf{w}_e$ is shown in the background.

V.   CONCLUSIONS

In this work, we investigated stabilization of unsteady flows by a reduced-order control algorithm based on the optimally-time dependent modes, a set of evolving modes that naturally track with directions of transient and persistent instabilities along a given trajectory. OTD control had already been used to suppress transient and asymptotic instabilities of a fixed point of the governing equations in [15], but the results presented therein pertained to small-amplitude disturbances and, hence, relied on the assumption that the dynamics of the system approximately obeyed the linearized equations. Thus, it was not clear how robust the proposed control algorithm was to disturbances with larger amplitude. Moreover, the authors in [15] assumed the OTD controller to be omniscient and omnipotent, which
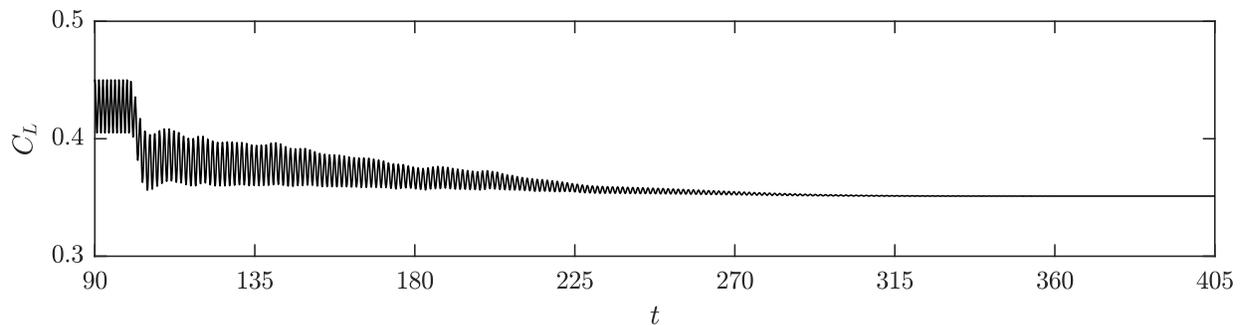
FIG. 14. For flow past a NACA 0012 airfoil with $\alpha = 10°$ at $Re = 1000$, detail of the time series of C_L for a trajectory initialized on the limit cycle and subject to localized OTD control with $r = 8$ and $\zeta = 3.4$ acting in the optimal subdomain identified in figure 13 ($x_c = 1.5L_c$ and $y_c = 0.05L_c$). Control is idle for $t < 100$ and active for $t \geq 100$.

is rarely the case in practice. They noted that one possible improvement to their approach would be to formulate an OTD control law that only acts in part of the physical domain. The present work aimed to address these two questions, namely, robustness and confinement of the control.

We began with an investigation of robustness of the control law proposed in [15]. Rather than considering small-amplitude perturbations, we assumed that the trajectory had already been ejected from the unstable fixed point, and was evolving on a long-time unsteady attractor. We applied OTD control to determine whether it was possible to annihilate the attractor and steer the trajectory towards the fixed point, notwithstanding that the latter may lie quite far from the attractor on which the trajectory initially evolves. We considered a low-dimensional system mimicking transition to turbulence, and three high-dimensional fluid flows for which the temporal regularity of the attractor in the absence of control ranged from time-periodic to chaotic. In all these cases, we found that OTD control was able to destroy the attractor and drive the trajectory towards the target fixed point. For the low-dimensional system and the time-periodic fluid flows, stabilization was achieved using the smallest possible OTD subspace as predicted by linear theory. For the chaotic system, however, we had to include a number of OTD modes larger than that prescribed by linearized theory. In passing, we proposed a modification of the original control law by Blanchard et al. [15] that eliminated temporal discontinuities in the control force.

We went on to formulate an OTD control law in which the OTD modes were computed in a subdomain of the physical domain of interest. This was done in recognition of the fact that computing the OTD modes in a subdomain yields a control force that is localized in space, which makes the approach more attractive from the standpoint of experiments. Computation of the OTD modes in a localized domain required specification of boundary conditions, and we argued that homogeneous Dirichlet boundary conditions were appropriate to perform comparison between various control subdomains. We also showed that the long-time average of the leading instantaneous OTD eigenvalue is a good indicator for selecting the location of the control subdomain once the extent of the latter has been decided. Interestingly, for the two bluff-body flows investigated, this indicator suggested that the control subdomain should be located in the near wake, no more than a few characteristic lengths behind the object. For these flows, localized OTD control was able to steer the trajectory towards the fixed point and stabilize the wake. Possible improvements of the localized OTD control strategy include state and OTD modes reconstruction using sparse measurements, and actuation on the object surface in the form of time-dependent boundary conditions.

We conclude with a few remarks on potential applications of OTD control in fluid flows, besides stabilization of a fixed point of the Navier–Stokes equations. First, we recall that the OTD modes have been used as precursors for extreme events in turbulent flows [22]. In principle, they could also be incorporated into control algorithms designed to suppress these extreme events, which would be a first step towards taming turbulence. One approach could be to transpose the control strategy proposed here to situations in which OTD control could prevent the system from executing large excursions from the mean state of the turbulent attractor. Second, we note that in the majority of flow control applications, it is not the whole state of the system that is of interest, but rather some observable, such as drag, lift or skin friction. In its current manifestation, the OTD framework applies to the phase space, but it could presumably be extended to the space of observables, merging with ideas from Koopman theory. This could lead to the formulation of reduced-order algorithms that specifically target instabilities of some observable without having to compute or reconstruct the full state. Such algorithms would pave the way for design of efficient and practical controllers for drag reduction in turbulent flows.

ACKNOWLEDGMENTS

---

[1] K. J. Åström and P. R. Kumar, "Control: A perspective," Automatica **50**, 3–43 (2014).

[2] S. Skogestad and I. Postlethwaite, *Multivariable Feedback Control: Analysis and Design* (Wiley New York, 2007).

[3] C. W. Rowley and S. T. M. Dawson, "Model reduction for flow analysis and control," Annual Review of Fluid Mechanics **49**, 387–417 (2017).

[4] P. Holmes, J. L. Lumley, and G. Berkooz, *Turbulence, Coherent Structures, Dynamical Systems and Symmetry* (Cambridge University Press, 1998).

[5] C. W. Rowley, "Model reduction for fluids, using balanced proper orthogonal decomposition," International Journal of Bifurcation and Chaos **15**, 997–1013 (2005).

[6] J.-N. Juang and R. S. Pappa, "An eigensystem realization algorithm for modal parameter identification and model reduction," Journal of Guidance, Control, and Dynamics **8**, 620–627 (1985).

[7] P. J. Schmid, "Dynamic mode decomposition of numerical and experimental data," Journal of Fluid Mechanics **656**, 5–28 (2010).

[8] J. L. Proctor, S. L. Brunton, and J. N. Kutz, "Dynamic mode decomposition with control," SIAM Journal on Applied Dynamical Systems **15**, 142–161 (2016).

[9] J. Guckenheimer and P. Holmes, *Nonlinear Oscillations, Dynamical Systems, and Bifurcations of Vector Fields* (Springer, Berlin and New York, 1983).

[10] J.-M. Chomaz, "Global instabilities in spatially developing flows: Non-normality and nonlinearity," Annual Review of Fluid Mechanics **37**, 357–392 (2005).

[11] V. Theofilis, "Global linear instability," Annual Review of Fluid Mechanics **43**, 319–352 (2011).

[12] S. L. Brunton and B. R. Noack, "Closed-loop turbulence control: progress and challenges," Applied Mechanics Reviews **67**, 050801 (2015).

[13] J. Kim and T. R. Bewley, "A linear systems approach to flow control," Annual Review of Fluid Mechanics **39**, 383–417 (2007).

[14] T. R. Bewley, "Flow control: New challenges for a new renaissance," Progress in Aerospace Sciences **37**, 21–58 (2001).

[15] A. Blanchard, S. Mowlavi, and T. P. Sapsis, "Control of linear instabilities by dynamically consistent order reduction on optimally time-dependent modes," Nonlinear Dynamics **95**, 2745–2764 (2019).

[16] B. R. Noack, K. Afanasiev, M. Morzyński, G. Tadmor, and F. Thiele, "A hierarchy of low-dimensional models for the transient and post-transient cylinder wake," Journal of Fluid Mechanics **497**, 335–363 (2003).

[17] P. J. Schmid, "Nonmodal stability theory," Annual Review of Fluid Mechanics **39**, 129–162 (2007).

[18] H. Babaee and T. P. Sapsis, "A minimization principle for the description of modes associated with finite-time instabilities," Proceedings of the Royal Society A **472**, 20150779 (2016).

[19] A. Wolf, J. B. Swift, H. L. Swinney, and J. A. Vastano, "Determining Lyapunov exponents from a time series," Physica D: Nonlinear Phenomena **16**, 285–317 (1985).

[20] A. Blanchard and T. P. Sapsis, "Analytical description of optimally time-dependent modes for reduced-order modeling of transient instabilities," (2019), to appear in *SIAM Journal on Applied Dynamical Systems*.

[21] H. Babaee, M. Farazmand, G. Haller, and T. P. Sapsis, "Reduced-order description of transient instabilities and computation of finite-time Lyapunov exponents," Chaos: An Interdisciplinary Journal of Nonlinear Science **27**, 063103 (2017).

[22] M. Farazmand and T. P. Sapsis, "Dynamical indicators for the prediction of bursting phenomena in high-dimensional systems," Physical Review E **94**, 032212 (2016).

[23] L. N. Trefethen, A. E. Trefethen, S. C. Reddy, and T. A. Driscoll, "Hydrodynamic stability without eigenvalues," Science **261**, 578–584 (1993).

[24] J. Dušek, P. Le Gal, and P. Fraunié, "A numerical and theoretical study of the first Hopf bifurcation in a cylinder wake," Journal of Fluid Mechanics **264**, 59–80 (1994).

[25] F. Giannetti and P. Luchini, "Structural sensitivity of the first instability of the cylinder wake," Journal of Fluid Mechanics **581**, 167–197 (2007).

[26] P. F. Fischer, J. W. Lottes, and S. G. Kerkemeier, "`nek5000` Web page," (2008), `http://nek5000.mcs.anl.gov`.

[27] E. Åkervik, L. Brandt, D. S. Henningson, J. Hœpffner, O. Marxen, and P. Schlatter, "Steady solutions of the Navier–Stokes equations by selective frequency damping," Physics of Fluids **18**, 068102 (2006).

[28] C. H. K. Williamson, "Vortex dynamics in the cylinder wake," Annual Review of Fluid Mechanics **28**, 477–539 (1996).

[29] S. V. Ershov and A. B. Potapov, "On the concept of stationary Lyapunov basis," Physica D: Nonlinear Phenomena **118**, 167–198 (1998).

[30] See Supplemental Material at [URL will be inserted by publisher] for supplemental movies referenced in the paper.

[31] D. F. Kurtulus, "On the unsteady behavior of the flow around NACA 0012 airfoil with steady external conditions at $Re = 1000$," International Journal of Micro Air Vehicles **7**, 301–326 (2015).

[32] P. M. Munday, *Active Flow Control and Global Stability Analysis of Separated Flow over a NACA 0012 Airfoil*, Ph.D. thesis, The Florida State University (2017).

[33] C. Foias, O. Manley, R. Rosa, and R. Temam, *Navier–Stokes Equations and Turbulence* (Cambridge University Press, 2001).

[34] N. Platt, L. Sirovich, and N. Fitzmaurice, "An investigation of chaotic Kolmogorov flows," Physics of Fluids A: Fluid Dynamics **3**, 681–696 (1991).

[35] G. J. Chandler and R. R. Kerswell, "Invariant recurrent solutions embedded in a turbulent two-dimensional Kolmogorov flow," Journal of Fluid Mechanics **722**, 554–595 (2013).

[36] M. Farazmand, "An adjoint-based approach for finding invariant solutions of Navier–Stokes equations," Journal of Fluid Mechanics **795**, 278–312 (2016).

[37] A. Peplinski, P. Schlatter, P. F. Fischer, and D. S. Henningson, "Stability tools for the spectral-element code Nek5000: Application to Jet-in-Crossflow," in *Spectral and High Order Methods for Partial Differential Equations* (Springer, 2014) pp. 349–359.

[38] S. J. Illingworth, "Model-based control of vortex shedding at low reynolds numbers," Theoretical and Computational Fluid Dynamics **30**, 429–448 (2016).

[39] A. Barbagallo, D. Sipp, and P. J. Schmid, "Closed-loop control of an open cavity flow using reduced-order models," Journal of Fluid Mechanics **641**, 1–50 (2009).

[40] G. Tadmor, O. Lehmann, B. R. Noack, and M. Morzyński, "Mean field representation of the natural and actuated cylinder wake," Physics of Fluids **22**, 034102 (2010).

[41] M. Bergmann, L. Cordier, and J.-P. Brancher, "Optimal rotary control of the cylinder wake using proper orthogonal decomposition reduced-order model," Physics of Fluids **17**, 097101 (2005).

[42] D. M. Luchtenburg, B. Günther, B. R. Noack, R. King, and G. Tadmor, "A generalized mean-field model of the natural and high-frequency actuated flow around a high-lift configuration," Journal of Fluid Mechanics **623**, 283–316 (2009).

[43] S. Ahuja and C. Rowley, "Low-dimensional models for feedback stabilization of unstable steady states," in *46th AIAA Aerospace Sciences Meeting and Exhibit* (2008) p. 553.

[44] G. C. Lewin and H. Haj-Hariri, "Reduced-order modeling of a heaving airfoil," AIAA journal **43**, 270–283 (2005).

[45] O. K. Rediniotis, J. Ko, and A. J. Kurdila, "Reduced order nonlinear Navier–Stokes models for synthetic jets," Journal of Fluids Engineering **124**, 433–443 (2002).

[46] K. Kwon and H. Choi, "Control of laminar vortex shedding behind a circular cylinder using splitter plates," Physics of Fluids **8**, 479–486 (1996).

[47] C. J. Doolan, "Flat-plate interaction with the near wake of a square cylinder," AIAA Journal **47**, 475–479 (2009).

[48] O. Marquet, D. Sipp, and L. Jacquin, "Sensitivity analysis and passive control of cylinder flow," Journal of Fluid Mechanics **615**, 221–252 (2008).

[49] P. J. Schmid and L. Brandt, "Analysis of fluid systems: Stability, receptivity, sensitivity," Applied Mechanics Reviews **66**, 024803 (2014).